

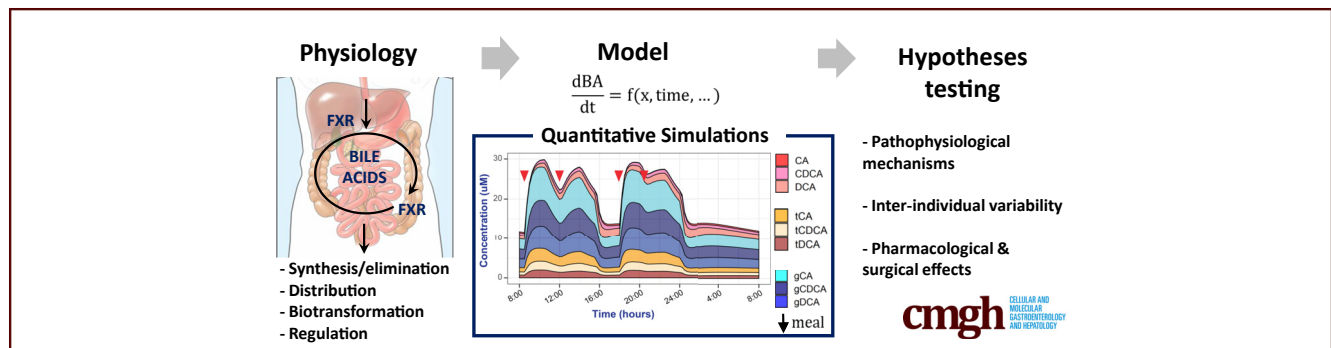
ORIGINAL RESEARCH

A Physiology-Based Model of Bile Acid Distribution and Metabolism Under Healthy and Pathologic Conditions in Human Beings



Veronika Voronova,¹ Victor Sokolov,¹ Amani Al-Khaifi,^{2,3,4} Sara Straniero,^{2,3} Chanchal Kumar,^{3,5} Kirill Peskov,^{1,6} Gabriel Helmlinger,⁷ Mats Rudling,^{2,3} and Bo Angelin^{2,3}

¹Department of Pharmacological Modeling, M&S Decisions, Moscow, Russia; ²Metabolism Unit, Endocrinology, Metabolism and Diabetes, Department of Medicine, ³Karolinska Institutet/AstraZeneca Integrated Cardio Metabolic Centre, Department of Medicine Huddinge, Karolinska Institutet, Karolinska University Hospital Huddinge, Stockholm, Sweden; ⁴Department of Biochemistry, College of Medicine and Health Sciences, Sultan Qaboos University, Muscat, Oman; ⁵Translational Science and Experimental Medicine, Research and Early Development, Cardiovascular, Renal and Metabolism, BioPharmaceuticals Research and Development, AstraZeneca, Gothenburg, Sweden; ⁶Computational Oncology Group, Sechenov First Moscow State Medical University of the Russian Ministry of Health, Moscow, Russia; ⁷Clinical Pharmacology and Safety Sciences, BioPharmaceuticals Research and Development, AstraZeneca, Boston, Massachusetts



SUMMARY

A physiological model capturing distribution and biotransformation of 3 major bile acids (cholic, chenodeoxycholic, and deoxycholic acids) was developed based on previous modeling works and used to simulate the effect of enterohepatic circulation perturbations on bile acid metabolism.

BACKGROUND & AIMS: Disturbances of the enterohepatic circulation of bile acids (BAs) are seen in a number of clinically important conditions, including metabolic disorders, hepatic impairment, diarrhea, and gallstone disease. To facilitate the exploration of underlying pathogenic mechanisms, we developed a mathematical model built on quantitative physiological observations across different organs.

METHODS: The model consists of a set of kinetic equations describing the syntheses of cholic, chenodeoxycholic, and deoxycholic acids, as well as time-related changes of their respective free and conjugated forms in the systemic circulation, the hepatportal region, and the gastrointestinal tract. The core structure of the model was adapted from previous modeling research and updated based on recent mechanistic insights, including farnesoid X receptor-mediated autoregulation of BA synthesis and selective

transport mechanisms. The model was calibrated against existing data on BA distribution and feedback regulation.

RESULTS: According to model-based predictions, changes in intestinal motility, BA absorption, and biotransformation rates affected BA composition and distribution differently, as follows: (1) inhibition of transintestinal BA flux (eg, in patients with BA malabsorption) or acceleration of intestinal motility, followed by farnesoid X receptor down-regulation, was associated with colonic BA accumulation; (2) in contrast, modulation of the colonic absorption process was predicted to not affect the BA pool significantly; and (3) activation of ileal deconjugation (eg, in patients with small intestinal bacterial overgrowth) was associated with an increase in the BA pool, owing to higher ileal permeability of unconjugated BA species.

CONCLUSIONS: This model will be useful in further studying how BA enterohepatic circulation modulation may be exploited for therapeutic benefits. (*Cell Mol Gastroenterol Hepatol* 2020;10:149–170; <https://doi.org/10.1016/j.jcmgh.2020.02.005>)

Keywords: Bile Acids; Farnesoid X Receptor; Cholesterol 7 α -Hydroxylase; Fibroblast Growth Factor-19; Physiology-Based Modeling.

The maintenance of an adequate pool of bile acids (BAs) in the enterohepatic circulation (EHC) is of critical importance for a number of physiological processes in healthy human beings, not only for ensuring appropriate absorption of food constituents but also for interaction with the environment including infectious agents such as the intestinal microbiota.¹ By influencing the elimination (both through direct biliary excretion and conversion to BAs) and absorption of cholesterol, modulation of the EHC provides major mechanisms for regulating not only lipid, but also carbohydrate and protein, metabolism.^{2–4} Disturbances of the BA EHC are involved in the pathogenesis of a number of clinically important conditions, such as malabsorption, dyslipidemia and atherosclerosis, chronic liver disease, and cholesterol gallstone disease.^{5–7}

Understanding how the concentration and composition of BAs are controlled in various portions of the EHC has improved over the past decades, including the recognition of BA-activated transcription factors such as the farnesoid-X receptor (FXR) and of selective BA transporters in liver and intestine.⁸ Activation of ileal and hepatic FXRs results in suppression of the activity of the rate-limiting enzymatic step of BA synthesis, cholesterol 7 α -hydroxylase (CYP7A1).⁹ Secretion of BAs from the hepatocyte into the bile canaliculi occurs through a set of BA transporters such as the bile salt export pump and organic anion transporting polypeptides (OATPs); meanwhile, other transporters, including the apical sodium-dependent bile acid transporter (ASBT) and organic solute transporters,¹⁰ are of major importance in the small intestine.

Although interference of BAs with the EHC through treatment with cholesterol-lowering BA-binding resins or natural BAs has been used extensively in therapeutic intervention efforts,^{11,12} the development of synthetic FXR agonists and antagonists as well as drugs influencing BA transporters¹³ has led more recently to the availability of new classes of drugs. These drugs are under evaluation for clinical conditions such as nonalcoholic steatohepatitis and cholestatic liver disease, as well as metabolic diseases such as diabetes, hyperlipidemia, and insulin resistance.^{2,14} In addition, the possible importance of BA-regulated signaling via circulating mediators such as fibroblast growth factor-19 (FGF-19) has become a subject of interest.

Given the complex network of mechanisms underlying regulation of BA synthesis, quantitative characterization of the composition and distribution of the BA pool should be relevant for understanding BA-associated disease. Mathematical modeling is a powerful instrument for the analysis of heterogeneous physiological and biological information issued from diverse experimental conditions and often is used to identify functional and interventional aspects of the system under study. Several models incorporating BA physiology and related aspects of EHC have been developed previously. Early work by Hofmann et al^{15,16} and Molino et al¹⁷ included a detailed mechanistic description of the dynamics of the major human BAs, cholic acid (CA), chenodeoxycholic acid (CDCA), and deoxycholic acid (DCA) in the EHC, hepatobiliary tract, and gastrointestinal tract. In more recent work, Guiastrennec et al¹⁸ developed and applied a nonlinear mixed-effects

model, with a simplified description of EHC, to study the effects of meal composition on the distribution of the total BA pool. Likewise, a mechanistic model by Sips et al¹⁹ has been used to identify determinants of BA pool composition. However, these models do not take into account FXR-dependent BA autoregulation, a necessary process to consider for accurate *in silico* reproduction of pathologic conditions.

In this original research, we developed a mechanistic model based on earlier work by Hofmann et al^{15–17} and augmented it with up-to-date information on pathophysiological regulations. The proposed model was thoroughly analyzed, validated, and subsequently applied to predict daily oscillations of the 3 main BAs (CA, CDCA, and DCA) in their conjugated and unconjugated forms in different organs, and to quantify the effect of BAs on FXR activation through plasma FGF-19. This model may further serve as a quantitative tool to test various hypotheses in the framework of BA-associated diseases.

Results

Model Reproduction of Experimental Data

A detailed description of the model development and the model structure is available in the Materials and Methods section, and the model schematics are summarized in Figure 1. The final model adequately captured distributions of total BAs, differences in fractions of individual BAs across organs, as well as the relationship between C4 and FGF-19 levels, as shown by goodness-of-fit plots and comparison of observed against predicted values (Figure 2).

The highest levels of BAs were predicted to be present in the biliary tract compartments (gallbladder and bile ducts), followed by the duodenojejunal and ileal tracts (Figure 2A). Because of the efficient ileal BA absorption and biotransformation, simulated average total colonic CA, CDCA, and DCA exposures were relatively small (400 $\mu\text{mol/L}$), in line with measurements obtained from fecal content.²⁰ Available experimental evidence suggested a BA level of 2–6 $\mu\text{mol/L}$ in feces.^{21,22} A balance between fast hepatic BA uptake and slow biliary BA flow resulted in a relatively high hepatic BA exposure (~ 30 nmol/g , or, equivalently, 60 $\mu\text{mol/L}$), in line with biopsy data.²³ A minor fraction of BAs reached the

Abbreviations used in this paper: ASBT, apical sodium-dependent bile acid transporter; BA, bile acid; CA, cholic acid; CDCA, chenodeoxycholic acid; CYP7A1, cholesterol 7 α -hydroxylase; DCA, deoxycholic acid; EHC, enterohepatic circulation; FGF-19, fibroblast growth factor-19; FXR, farnesoid X receptor; gCA, glycine-conjugated cholic acid; gCDCA, glycine-conjugated chenodeoxycholic acid; gDCA, glycine-conjugated deoxycholic acid; NTCP, sodium-taurocholate cotransporting polypeptide; OATP, organic anion transporting polypeptide; ODE, ordinary differential equation; tCA, taurine-conjugated cholic acid; tCDCA, taurine-conjugated chenodeoxycholic acid; tDCA, taurine-conjugated deoxycholic acid; uBA, unconjugated bile acid; uCA, unconjugated cholic acid; uCDCA, unconjugated chenodeoxycholic acid; uDCA, unconjugated deoxycholic acid.

 Most current article

© 2020 The Authors. Published by Elsevier Inc. on behalf of the AGA Institute. This is an open access article under the CC BY-NC-ND license (<http://creativecommons.org/licenses/by-nc-nd/4.0/>).

2352-345X

<https://doi.org/10.1016/j.jcmgh.2020.02.005>

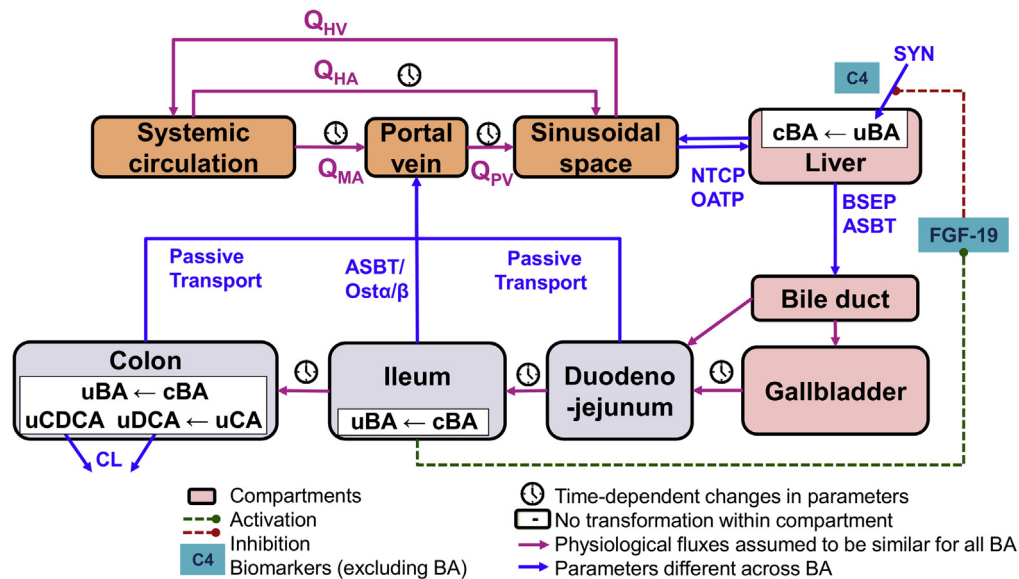


Figure 1. Proposed model structure. uCA and uCDCA are synthesized in the liver and undergo conjugation with glycine or taurine together with recirculated uCA, uCDCA, and uDCA. Newly conjugated gCA, tCA, gCDCA, tCDCA, gDCA, and tDCA, together with recycled conjugated BA, are secreted into the bile ducts from where they flow directly into the duodenojejenum or are stored in the gallbladder. Food intake is followed by gallbladder contraction and additional BA release into the duodenojejenum. Conjugated BAs are transported to lower regions of the gastrointestinal tract, where they are deconjugated or dehydroxylated. A minor fraction of BAs is excreted in feces. After entering into the portal vein, BAs flow into the sinusoidal space where they can be cleared by the liver or enter the systemic circulation via the hepatic vein. From the systemic circulation, BAs can return to the portal space via the mesenteric or hepatic artery. Note that additional compensatory BA fluxes activated in cholestatic liver disease (eg, cholehepatic shunt, renal BA excretion) were not considered in the model. BSEP, bile salt export pump; CL, clearance.

systemic circulation, ensuring fasting serum BA levels of approximately 2–3 $\mu\text{mol/L}$.⁹

Predicted amounts of CA in the systemic plasma were lower than in the portal circulation owing to efficient hepatic CA clearance.²⁴ The low presence of primary BAs (CA and CDCA) in the colon was the result of a high abundance of intestinal microbiota. Proportions of (un)conjugated BAs differed among compartments (Figure 2C). Only conjugated BAs were present in the biliary tract and the duodenojejenum, while the proportion of unconjugated forms increased toward the lower intestinal regions. An overprediction could be observed in the amount of conjugated BAs in the ileum, possibly owing to the simplified representation of the ileum as a single compartment, whereas experimental evidence would suggest an uneven distribution of conjugated BAs along the small intestine.²⁵ Most BAs in the portal circulation were present in their conjugated forms, while respective amounts in the systemic circulation were lower owing to higher hepatic uptake.⁹

The relationship between FXR modulation and BA synthesis was represented in the model as a dynamic interplay between plasma FGF-19 and C4 concentrations (Figure 2B). Limited daily oscillations in plasma C4 and FGF-19 driven by postprandial activation of transintestinal BA fluxes were observed under normal conditions. In contrast, model-based predictions on the effects of administration of a nonsteroidal FXR agonist suggested an up to 15-fold increase in FGF-19 and an almost complete depletion of C4, in line with experimental data obtained after treatment with Px-102 (Phenex Pharmaceuticals AG, Heidelberg, Germany).²⁶

Simulations of Daily BA Dynamics in Healthy Subjects

Upon successful verification, the model was used to predict daily time profiles of BAs in different organs, plasma FGF-19, and C4 oscillations, and BA-related rates and fluxes across compartments (Figure 3), to identify key determinants of BA distribution following the experimental design⁹ with meals given at 8:30, 13:00, 18:00, and 20:30.

The model predicted a sharp ~2-fold increase in systemic BA exposure, driven primarily by conjugated BAs after food intake, which is in agreement with experimental evidence.⁹ Similar changes over time in BA levels were observed in the systemic circulation, the portal vein, and the liver (Figure 3A), as follows from the fast hepatic BA clearance and high perfusion rate of the liver, to ensure rapid BA equilibration between these compartments (Figure 3C). In contrast, BA distribution within the biliary and the gastrointestinal tracts was determined by relatively slow processes such as bile flow and intestinal and colonic food fluxes, resulting in different BA abundancies in the respective compartments (Figure 3A). The release of bile from the gallbladder after a meal and the subsequent increase in the transintestinal BA flux resulted in an approximately 50% increase in plasma FGF-19 levels and inhibited BA synthesis, as seen from C4 levels (Figure 3B).

Portal BA concentration was sensitive to changes in ileal BAs because the ileum is the major site for BA absorption. Despite unconjugated BAs having a higher permeability vs conjugated BAs,²⁷ most BAs absorbed in the ileum were

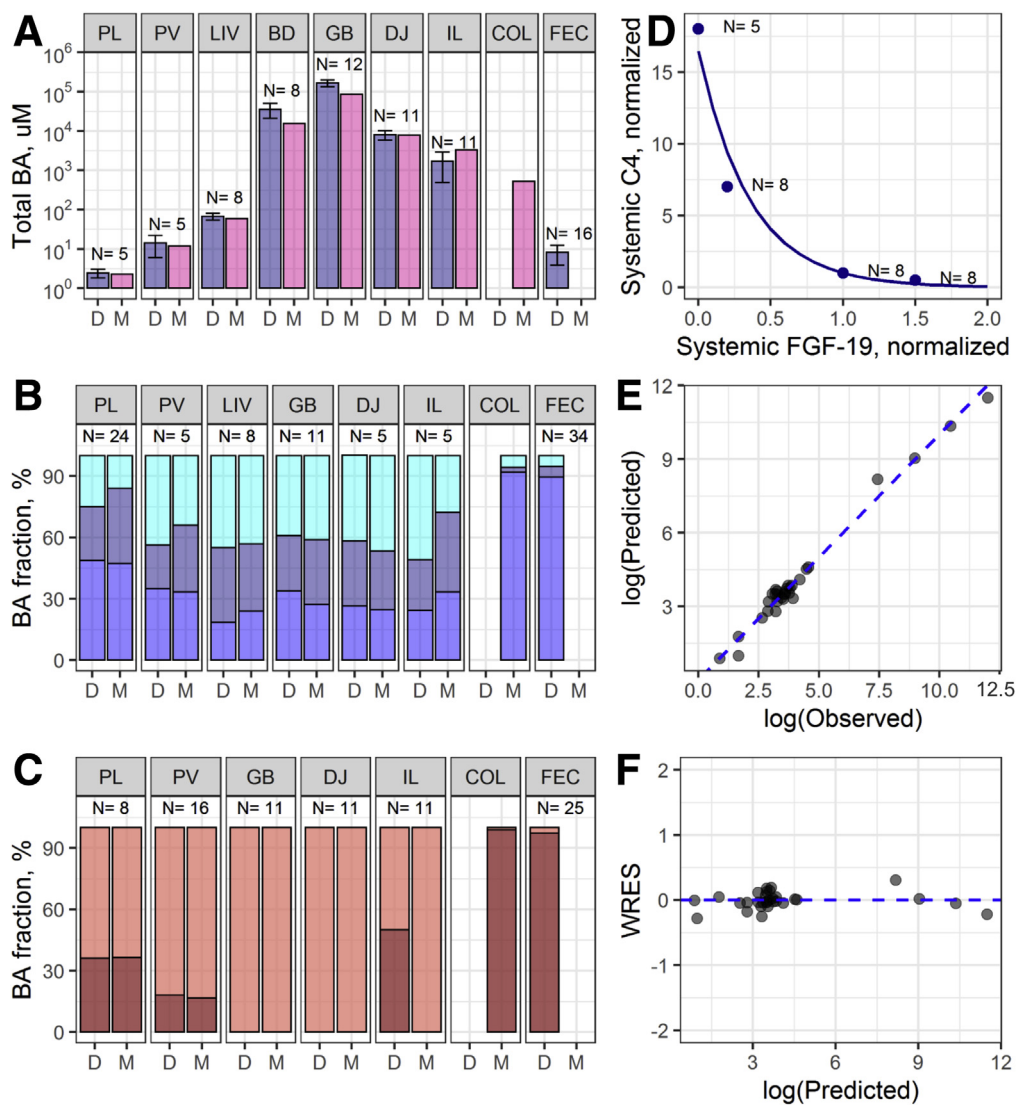


Figure 2. Model reproduction of experimental data.

(A) Total BA levels across organs; experimental data shown as mean values; error bars denote 95% CIs. (B) Individual and (C) unconjugated BA fractions in different organs (BA species are identified by color, as follows: CA, light blue; CDCA, dark blue; DCA, medium blue; unconjugated BA, brown; conjugated BA, light pink). (D) Relationship between systemic FGF-19 and C4 levels (dots indicate experimental data, line indicates model predictions). Details on experimental data are reported in Table 3. (E) Observations vs model predictions: the straight line represents a perfect agreement between experimental data and calculated values. (F) Plot of weighted residuals. N denotes the number of subjects in each experiment. BD, bile duct; COL, colon; D, experimental data; DJ, duodenojejunum; FEC, feces; GB, gallbladder; IL, ileum; LIV, liver; M, model predictions; PL, plasma; PV, portal vein; WRES, weighted residuals.

conjugated. In contrast, only unconjugated BAs were absorbed from the colonic lumen. This discrepancy can be explained by differences in BA abundance between compartments because ileal BAs are primarily in conjugated forms while colonic BAs are mostly unconjugated. Overall CA absorption from the jejunum and colon was negligible, whereas the proportion of CA in the portal vein reached 50% of the total as a result of ileal absorption (Figure 3C). Colonic permeabilities for CDCA and DCA were similar,²⁸ although DCA absorption was higher vs CDCA owing to a greater fraction of DCA available in the colon.

Hepatic BA uptake predominantly mirrors ileal BA absorption and serves as a key source of BAs in the liver, with a rate of 400–1200 $\mu\text{mol/h}$, vs a de novo primary BA synthesis rate of 46 $\mu\text{mol/h}$ (or, equivalently, 540 mg/day) (Figure 3C). Primary BAs are synthesized in the unconjugated form, whereas most BAs taken up by the liver are conjugated, as a result of greater availability of conjugated BAs in the portal region and greater fractional

hepatic uptake of conjugated vs unconjugated BAs.²⁴ The model predicted an increase in postprandial DCA synthesis after accumulation of its precursor, CA, in the colon, whereas the postprandial de novo CA synthesis was suppressed in response to FXR activation by transintestinal BA flux. In the fasting condition, BA secretion from the liver was set to be equal to the hepatic uptake of BAs to ensure near-constant BA levels in the liver in the absence of food intake.

Simulations of EHC Variability Effects on BA Pool Size and Composition

The model was used further to evaluate the sensitivity of BA levels toward quantities of BA distribution and biotransformation parameters within the gastrointestinal tract. For this purpose, model parameters were varied one by one within predefined, physiologically plausible ranges, with subsequent prediction of average daily concentrations

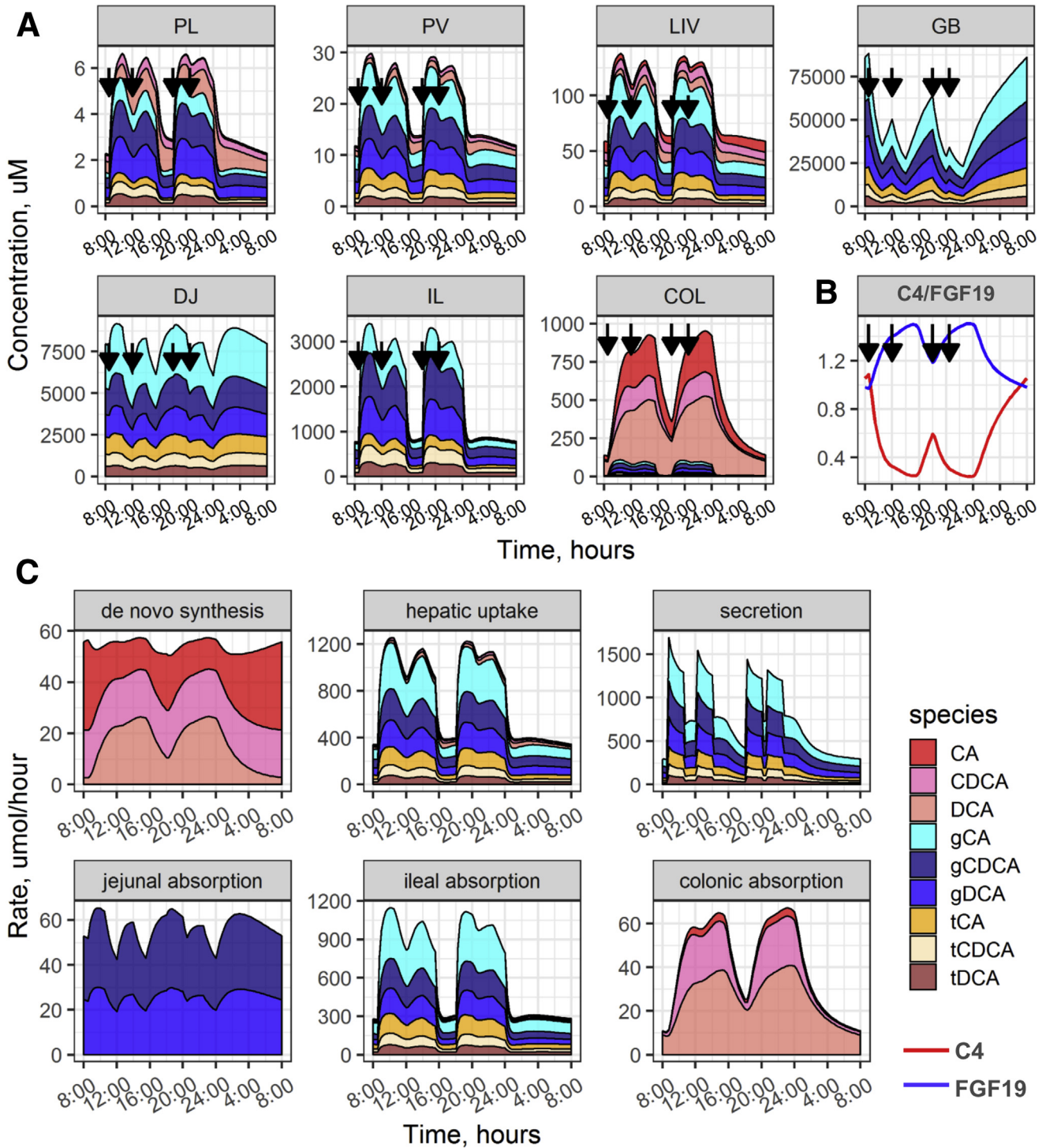


Figure 3. Model simulations of (A) daily dynamics of individual BAs in different compartments, (B) C4 and FGF-19 dynamics in the systemic circulation, and (C) reaction rates of BA synthesis, biotransformation, and distribution. COL, colon; DJ, duodenojejunum; GB, gallbladder; IL, ileum; LIV, liver; PL, plasma; PV, portal vein

of individual BAs in the systemic circulation and in the colon (Figure 4). Parameters of absorption and gastrointestinal motility were varied over a $\pm 50\%$ range,⁶ whereas parameters of microbiota activity were changed over a much wider range of 10%–1000%, assuming high interindividual variability in microbiota activity.

Changes in BA pool size and composition after changes in absorption rates were found to be dependent on the particular compartment where the alterations would take place (Figure 4A and B). Modulation of duodenojejunal absorption did not interfere significantly with BA distribution. In contrast, with the ileum representing the main route for

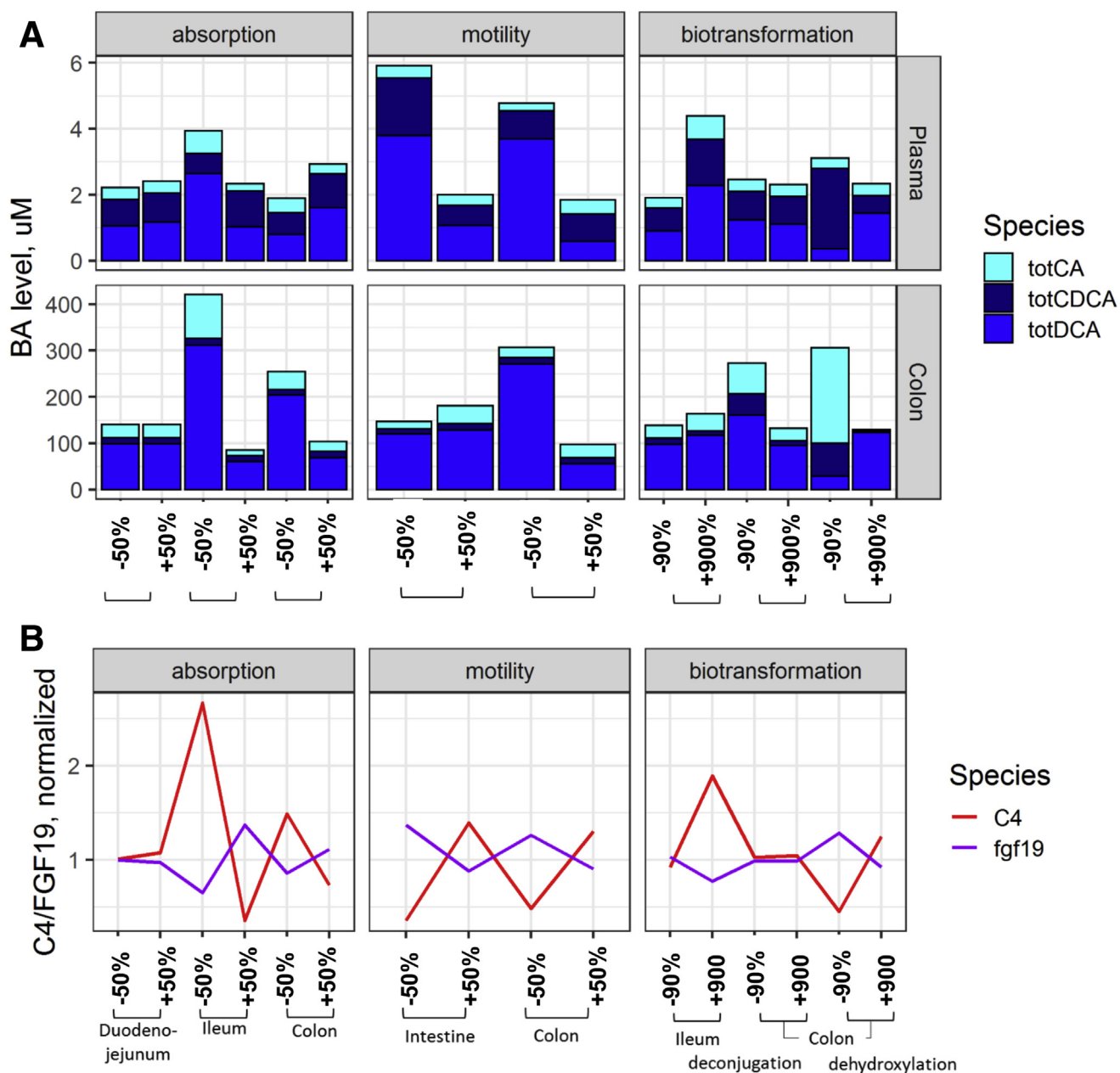


Figure 4. Effects of a $\pm 50\%$ parameter change in daily average values on individual BA levels (A) in systemic plasma and (B) in the colonic space. (C) Systemic C4, FGF-19 normalized levels. Species are identified by color: CA, light blue; CDCA, dark blue; DCA, medium blue; FGF-19, red; C4, violet. tot, total.

BA absorption, a decrease in transintestinal flux in the ileum strongly affected both the composition and distribution of the overall pool of BAs. Thus, a decrease in ileal BA absorption was followed by a reduction in transhepatic BA flux, a decrease in plasma FGF-19, and a compensatory activation of CA synthesis, thereby preserving the BA pool (Figure 4C). At the same time, colonic CA input increased, leading to the accumulation of CA and its metabolite DCA in the colon (Figure 4B). These changes resulted in increased systemic exposure of CA and DCA and reduced exposure of CDCA. Because ileal BA absorption is rapid even under normal conditions, a further increase did not result in an additional increase of the circulating BA pool

but did stimulate FXR activation followed by a reduction of CA synthesis (Figure 4C). The synergy between increased ileal CA absorption and a reduction of CA synthesis caused a decrease in colonic CA input, which eventually led to a decrease in DCA synthesis. Alterations of BA absorption in the colon affected mainly the DCA pool because the colon is the primary site for absorption of de novo synthesized DCA, and introduced minor perturbations to the CDCA pool. Increases in the abundance of both DCA and CDCA were associated with a compensatory decrease in BA synthesis (Figure 4C).

An acceleration of intestinal motility reduced ileal BA exposure, thereby leading to decreased absorption of BAs,

reduced BA levels in the systemic circulation, and stimulated BA synthesis (Figure 4A and C). In addition, it was associated with increased availability of CA in the colon, resulting in accelerated DCA production. In contrast, acceleration of colonic motility correlated negatively with the presence of DCA, implying that the lower CA exposure in the colon resulted in lower rates of DCA production.

The rate of ileal BA deconjugation correlated positively with both unconjugated and total BA levels in the systemic circulation. Interestingly, in such a setting, an increase in the transintestinal BA flux was not followed by FXR activation, given that the potency for FXR of unconjugated BAs is lower compared with the conjugated ones.²⁹ Deconjugation of BAs in the colon generally is fast, and hence a further increase would not affect the overall BA pool, whereas a decrease in colonic deconjugation should lead to an accumulation of BAs in the colon because conjugated BAs possess poor permeability properties. Decreases in both colonic deconjugation and dehydroxylation resulted in decreased DCA levels. Reduced colonic dehydroxylation led to an increase in plasma CDCA, but not CA, because CDCA may be absorbed in the colon, unlike CA.

Simulations of BA Malabsorption Treatment With an FXR Agonist

After a rigorous sensitivity analysis of the model toward various changes in BA fluxes and biotransformation rates, we analyzed the impact of EHC perturbations on BA metabolism by simulating BA-induced diarrhea and other pathologic states.

To investigate the role of FXR signaling in the pathogenesis of BA-induced diarrhea and to evaluate the effects on BA distribution induced by pharmacologic FXR stimulation, 2 parameters characterizing ileal BA absorption and BA-dependent FXR activation were varied over a broad range of values. Ileal absorption was varied between the healthy state (default value) and a complete absence thereof, as found in patients who have undergone ileostomy.⁵ Another parameter reflecting pharmacologic (BA-independent) FXR activation was varied, to mimic the FGF-19 increase in response to treatment with a nonsteroidal FXR agonist.³⁰

As shown in Figure 5A, a reduction in ileal BA absorption resulted in up to a 16-fold increase in BA synthesis, followed by the accumulation of BAs in the colon (Figure 5B). A 50% reduced transintestinal BA flux was associated with an increase in colonic BA concentration up to 3 mmol/L, a level sufficient to induce diarrhea.²⁸ The model predicted increases in both CA and DCA pools in the systemic circulation (Figure 5C), whereas CDCA levels remained unchanged (Figure 5D). Pharmacologic activation of FXR markedly reduced BA synthesis, preventing the accumulation of BAs in the colon. The optimal dose of the FXR agonist required to maintain colonic BAs below the 3 mmol/L threshold was dependent on the severity of BA malabsorption. However, even for patients with severe malabsorption (eg, ileostomy), FXR activation within physiological ranges was deemed sufficient to prevent BA-induced diarrhea.

Simulations of Cholecystectomy

The model was used to predict the change in BA concentrations over time in patients who underwent surgical interventions, such as cholecystectomy. Under normal conditions, the BA pool is stored in the gallbladder and released into the gastrointestinal tract in response to meal ingestion. In cholecystectomized patients, the gallbladder is removed, and the BA pool constantly passes down the intestine, which is associated with increased BA biotransformation by gut microbiota, leading to secondary BA accumulation.³¹ In some patients, cholecystectomy is followed by an increase in intestinal transit time and in small intestine bacterial overgrowth³²; these also may lead to secondary BA increase.

The state of cholecystectomy was reproduced in the model by setting the BA flux from the bile ducts to the gallbladder to zero, with or without an increase in the intestinal deconjugation rate. Daily plasma BAs, FGF-19 and C4, as well as daily average BA levels across the various organs, were simulated (Figure 6).

Based on model predictions, daily meal-driven BA oscillations were preserved in cholecystectomized patients, in agreement with experimental observations.³³ In such a setting, BAs are stored in the biliary tree and upper intestine; they transit to the lower gastrointestinal regions in response to food intake, as a consequence of increased intestinal motility. The predicted and observed magnitude of postprandial BA and FGF-19 changes were lower in cholecystectomized patients vs healthy subjects (Figure 3A and B).³³

Simulations of Short-Term Fasting

Short-term fasting was associated with systemic 50% BA and FGF-19 decrease and a 2-fold C4 increase.³⁴ This state was reproduced in the model by nullifying all meal-induced changes. Model-based predictions indicated an accumulation of BAs in the gallbladder resulting from the absence of meal-induced gallbladder emptying and the activation of BA synthesis under decreased intestinal BA levels (Figure 7). The DCA fraction was reduced as a result of a decreased input of BAs to the colon.

Discussion

Numerous hypotheses have linked EHC variability or perturbations to individual differences in BA metabolism and, consequently, the pathogenesis of multiple gastrointestinal disorders. Despite a substantial amount of diverse experimental information, large knowledge gaps remain. First, BAs typically are measured in the systemic circulation or in fecal samples, while the available information on BA levels within EHC compartments is sparse, given challenges of experimental measurements and access. Second, experimental designs required to test specific hypotheses cannot always be performed because of ethical considerations. In addition, many of the physiological processes considered here are known to vary considerably among individuals, including gastrointestinal transit times, expression levels of various transporters, microbiota compositions, and so forth.

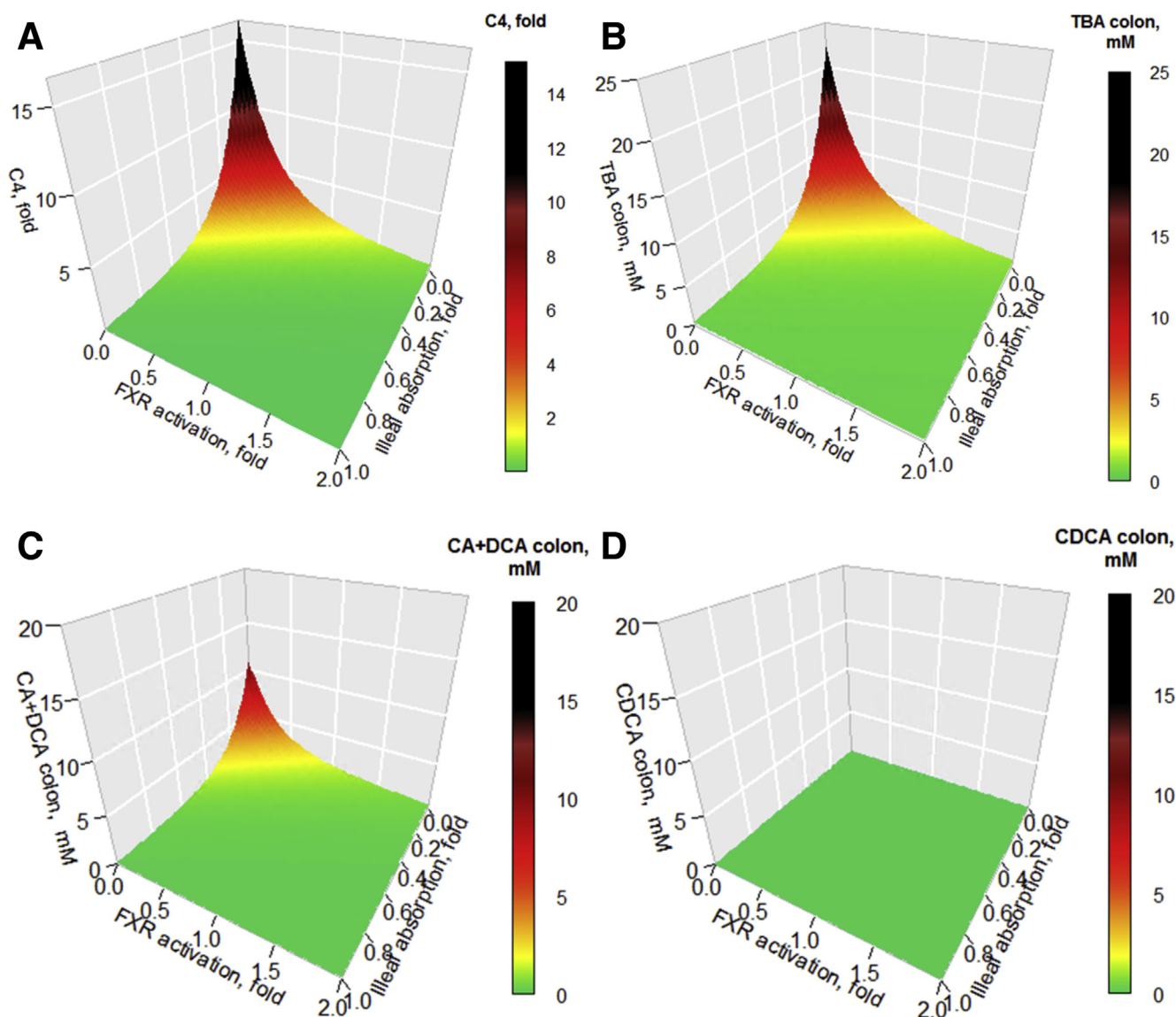
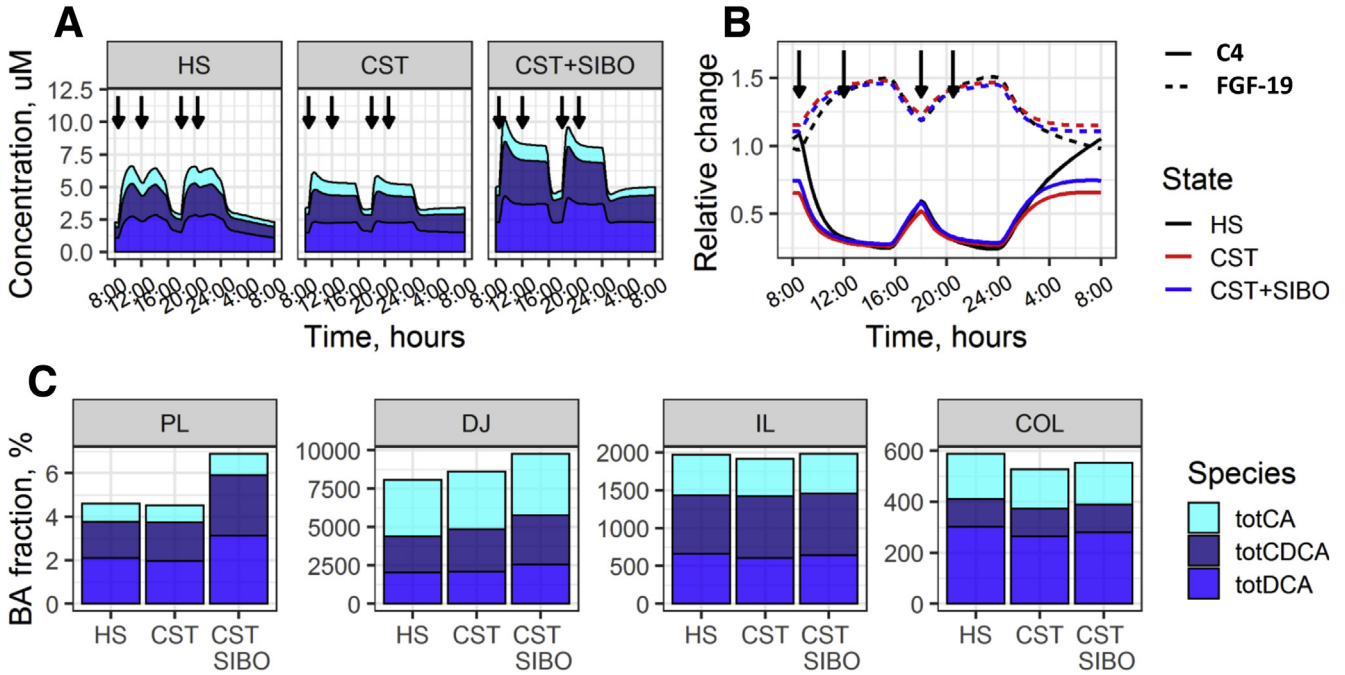


Figure 5. Effects of pharmacologic FXR activation and efficiency of ileal BA absorption on (A) normalized C4 levels in the systemic circulation, (B) total BAs, (C) sum of CA and DCA, and (D) DCA concentration within the colon. Color reflects the severity of colonic BA accumulation: BA concentrations that may induce water secretion are marked with yellow. TBA, total BA.

Such differences will result in significant interindividual variability in plasma BA profiles.⁹ This multifactorial nature of systemic plasma BA measurements complicates the identification of key factors that regulate BA pool distribution and composition. In their recent work, Fiamoncini et al³⁵ addressed this question by using a mixed-design analysis of a variance model exploiting host genome and microbiota data, in addition to systemic plasma BA profiles. However, interindividual variability is determined not only genetically, numerous additional factors, environmental and physiological, may contribute to the variability in BA pool size and composition.

Physiology-based modeling represents a powerful approach that allows for a rational integration of diverse experimental data into a single quantitative framework, which then may be used to analyze the behavior of

multiplexed biology and physiology over time, under normal and pathologic conditions, as well as after pharmacologic interventions. The model also may generate missing information within existing data and predict the system's behavior by extrapolating beyond existing data. The mathematical representation of the system (eg, inclusion of key processes, metabolites, model assumptions) was first framed based on the aims of the modeling study, the availability of experimental data, and current knowledge in the field. Here, we used a physiologically based mechanistic model to explore the distribution of BAs within the EHC under various normal and pathologic conditions and to investigate the effects of FXR-mediated BA autoregulation. As a basis for the model, we built on the pioneering work of Hofmann et al^{15,16} and Molino et al¹⁷ and incorporated additional mechanisms, including FXR-dependent regulation



of CYP7A1 activity, time-dependent variation of intestinal microbiota activity, and colonic absorption of primary BAs.^{36–38} We then performed simulations to predict individual BA levels within organs and tissues, using different model parameter values to mimic various EHC

perturbations. A related modeling study recently was reported by Sips et al.¹⁹ There are, however, notable differences between their approach and ours, as follows: (1) FXR-mediated regulation of CYP7A1 was explicitly considered in the current study, given its importance in ensuring

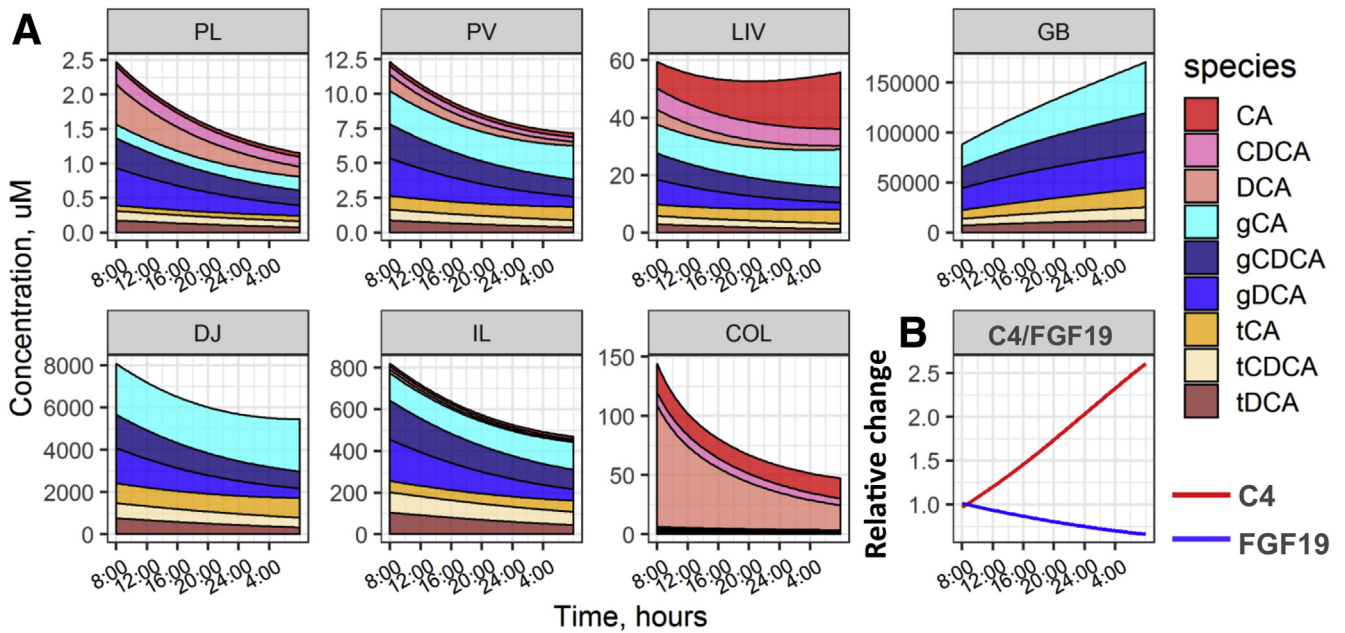


Figure 7. Model simulations of (A) daily dynamics of individual BA in different compartments, and (B) C4 and FGF-19 dynamics in the systemic circulation of subjects undergoing 24-hour fasting. COL, colon; DJ, duodenojejunum; GB, gallbladder; HS, healthy subjects; IL, ileum; LIV, liver; PL, plasma; PV, portal vein.

BA homeostasis; (2) a simpler representation of BA distribution within intestinal and colonic spaces was used here, which allowed for a reduction in the number of parameters to be estimated, while being less detailed in terms of BA distribution description along the gastrointestinal tract; and (3) the design of the sensitivity analysis in the present model was based on hypotheses and knowledge discussed extensively within the existing literature; in addition, ranges of parameter values were set to reflect the actual variability observed within experimental data. This resulted in our use of ranges of parameter values related to BA distribution and biotransformation, in contrast to an unspecified range of parameters used in the study by Sips et al.¹⁹ Such differences in modeling approaches complement each other, eventually providing an increasingly complete picture of BA physiology and pathophysiology.

In the present study, we first simulated BA distribution within the EHC of a typical healthy subject and quantified the impact of different variations of BA distribution (Figures 3 and 4). Under healthy conditions, more than 95% of secreted BAs are reabsorbed during each cycle in the EHC, resulting in a daily BA pool renewal rate of approximately 30%,³⁹ hence reabsorption from the gastrointestinal tract is crucial for maintaining the BA pool. We thus hypothesized variability in this process to be an important factor affecting BA distribution. Uneven reabsorption of individual BAs from different regions of the gastrointestinal tract has been observed, presumably owing to different epithelial wall permeabilities for different BA molecular species across intestinal regions, but also owing to variable BA composition along the intestinal tract. BA absorption starts already in the duodenojejunum, with at least 25% of CDCA and DCA conjugates being reabsorbed in that segment,⁴⁰ presumably by passive diffusion and via OATP3.⁴¹ An analysis by Fiamoncini et al³⁵ showed that variability in OATP3 expression may contribute to variability in postprandial plasma BA dynamics, whereas our analysis showed a small impact of duodenojejunal variability on daily average plasma BA levels. This may point to a compensatory increase in ileal BA absorption, preventing BA pool reduction, as detected by delayed BA absorption.

The ileum is the key site for BA absorption and, in particular, the dominant route for CA absorption, owing to its less efficient passive uptake.²⁸ Less than 5% of BAs escape ileal absorption each time they pass through the small intestine, moving on to the colon where they undergo biotransformation and conversion to secondary BAs such as DCA. Thus, modulation of colonic absorption is predicted to affect mainly the pool of secondary BAs. In contrast to ileal BA absorption, a decrease in colonic BA absorption is followed by mild FXR activation variations, owing to changes in the DCA pool size and subsequent changes in the transintestinal DCA flux.

Based on accumulating experimental and clinical evidence, variability in microbiota activity also may affect the BA pool. For example, preclinical data suggest that bacterial overgrowth in the small intestine may be associated with an increase in BA pool size.⁴² At the same time, a decrease in colonic deconjugation or dehydroxylation efficiency was

predicted to shift BA composition from secondary to primary species, which has been observed in subjects treated with antibiotics.⁴³

Finally, in the present study, we performed a theoretical exercise invoking simulations of colonic and systemic BA levels, using a range of parameter values for FXR activation and transintestinal BA flux, to mimic BA malabsorption conditions. Based on model simulations, FXR downregulation appeared to be crucial for colonic BA accumulation in patients with reduced transintestinal BA flux and, hence, restoration of FXR action with an agonist should be followed by a reduction in colonic BA input below levels associated with BA-induced water secretion. On the other hand, model-based simulations indicate that FXR activation may be followed by a pronounced reduction in the BA pool, which may result in fat malabsorption and, consequently, steatorrhea and fatty acid-induced diarrhea.⁴⁴

Although the model allowed us to investigate the potential impact of EHC perturbations on BA distribution, it is important to point out certain model limitations. Despite emerging experimental data, knowledge gaps do remain, making it challenging to represent the system in a fully mechanistic fashion. For example, estimating the contribution of different transporters involved in hepatocellular and cholangiocellular BA import/export is complex and would require simultaneous *in vivo* measurements of multiple transporter capacities. Another mechanistic challenge relates to uneven spatial distribution of the microbiota and the related activity along the lower regions of the gastrointestinal tract. Thus, although informative with respect to a subject's microbiome, data on fecal microbiota composition are not sufficient to provide the needed information on BA biotransformation in specific intestinal regions.

Finally, several mechanisms are involved in the regulation of BA synthesis, including intestinal FXR activation, mirrored by plasma FGF-19 changes, as well as direct hepatic FXR activation by BA.⁴ The latter pathway, however, was not explicitly considered in the model, given insufficient information to identify corresponding model parameters.

Despite these aforementioned limitations, the proposed model provides valuable insights into various aspects of BA physiology and represents a quantitative tool to support further explorations of physiological and pharmacologic regulations of human BA metabolism, including explorations of cholesterol and lipoprotein metabolism modulation in the treatment and prevention of significant medical conditions.

Materials and Methods

The development of a quantitative systems pharmacology model of BA distribution and metabolism was performed in several steps. First, a thorough review of the available knowledge and open-source data on BA distribution and metabolism was performed, with a subsequent compilation into a biological rationale. On a second step, existing mathematical representations of BA physiology were reviewed. Studies by Hofmann et al^{15,16} and Molino et al¹⁷ were selected as a basis for further model development because they were consistent with the current study

objectives and included a physiologically relevant description of BA distribution. These models subsequently were structured into a single modeling framework, which was updated further based on current knowledge (eg, with the introduction of FXR-mediated BA synthesis regulation).

Biological Rationale for the Proposed Mathematical Model Structure

The final model consisted of a set of ordinary differential equations representing synthesis, elimination, and distribution of unconjugated (u), and glycine- (g) or taurine-conjugated (t) CA, CDCA, and DCA (including unconjugated cholic acid [uCA], unconjugated chenodeoxycholic acid [uCDCA], unconjugated deoxycholic acid [uDCA], glycine-conjugated cholic acid [gCA], glycine-conjugated chenodeoxycholic acid [gCDCA], glycine-conjugated deoxycholic acid [gDCA], taurine-conjugated cholic acid [tCA], taurine-conjugated chenodeoxycholic acid [tCDCA], and taurine-conjugated deoxycholic acid [tDCA]) within the systemic and enterohepatic circulations, as well as their autoregulation via FXR, mirrored by FGF-19 and C4 changes in plasma. Experimental data on these processes were collected from multiple publicly available sources and are summarized in this section to provide a biological rationale for the proposed model structure.

De novo synthesis of primary BAs (CA and CDCA) occurs in the liver and is performed via the classic/neutral (CYP7A1-mediated) or the alternative/acidic (involving steroid 7α -hydroxylase [CYP7B1] and 24-hydroxycholesterol 7α -hydroxylase [CYP39A1]) pathways. Although CA is produced mainly via the classic pathway, the alternative pathway (contributing 10%–20% of the total in human beings) results predominantly in CDCA formation.^{45,46} In the liver, newly synthesized BAs are conjugated with taurine or glycine and secreted into the bile across the canalicular membrane. This process is a rate-limiting step of bile formation and is mediated mainly by the bile salt export pump (BSEP).⁴¹ Upon entering the biliary tree, BAs either are excreted directly into the intestine via common bile ducts, ensuring fasting BA secretion, or stored in the gallbladder and released in response to meal ingestion in a caloric-dependent manner (stimulated BA secretion).¹⁵

After release into the intestine where they contribute to micellar solubilization and absorption of dietary fat and vitamins, BAs are propagated to the ileum and colon. Absorption of dihydroxy BAs (CDCA and DCA) starts already in the jejunum and contributes approximately 15% to total BA absorption⁴⁰; it is mediated by passive nonionic diffusion²⁷ or possibly by transport systems, including the ASBT and the OATP.⁴⁷ A major fraction of BAs is absorbed efficiently in the lower small intestine by active transport (ASBT/organic solute transporters α/β),⁴⁶ and to some extent by passive diffusion. Only a minor fraction of BAs (approximately 5%) enters the colon, from where it is absorbed passively or excreted with feces.³⁹

BAs undergo transformations by gut microbiota within the gastrointestinal tract. These include deconjugation by various bacterial species,³⁹ starting in the ileum, with most

BAs being deconjugated in the colon.²⁵ Deconjugated primary bile acids undergo 7α -dehydroxylation by *Clostridium* bacteria, resulting in secondary BA formation (DCA from CA and lithocholic acid from CDCA). Ursodeoxycholic is formed from CDCA through additional epimerization from CDCA. Reabsorbed secondary BAs may be reabsorbed and recirculated together with primary BAs.³⁹

Reabsorbed BAs enter the portal circulation and are then cleared efficiently by the liver. Hepatic bile salt uptake occurs against a concentration gradient and is mediated by several transport systems, including sodium-taurocholate cotransporting polypeptide (NTCP) and OATPs.^{10,41} Because of the high affinity of binding of BAs to plasma proteins, particularly albumin, its dissociation to free form represents an important step for hepatic uptake.⁴¹ Approximately 15% of portal BAs are not cleared by the liver²⁴ and instead enter the systemic circulation to return to the hepatoportal region via hepatic or mesenteric arteries.¹⁵

Gallbladder emptying is not the only factor determining daily fluctuations in the BA pool. It has been shown that diurnal BA rhythms are preserved in cholecystectomized patients.³³ This can be explained by gastrointestinal motility modulation, as well as by an increased hepatoportal circulation postprandially.^{9,15} Numerous studies also have shown that the composition of circulating BAs is not constant during the day. It recently was shown that the proportion of unconjugated BAs increases during the night, which may be the result of diurnal oscillations in ileal microbiota activity,⁹ in line with observations by Thaiss et al,³⁷ who showed that the activity of specific microbial species undergoes diurnal oscillations influenced by feeding rhythms.

The meal-induced increase in transintestinal BA flux is associated with an activation of the ileal FXR, resulting in the release of FGF-19 into the portal circulation. This, in turn, activates fibroblast-growth factor receptor-4 in complex with β -Klotho on hepatocytes, which initiates suppression of CYP7A1. Portal venous BAs taken up by the liver also can suppress CYP7A1 via their activation of hepatic FXR.²⁶

Brief Description of the Original Models and Applied Modifications

A detailed description of the models by Hofmann et al^{15,16} and Molino et al¹⁷ was described previously. In summary, all models feature a similar structure and include the following compartments: (1) portal (hepatic artery and vein, portal vein, sinusoidal space) and systemic circulation; (2) hepatobiliary tract (liver, bile duct, and gallbladder); and (3) gastrointestinal tract (upper and lower intestine and colon). The models are represented by ordinary differential equations (ODEs) describing the amounts of individual unconjugated, glycine-conjugated, or taurine-conjugated CAs (uCA, gCA, and tCA),¹⁵ CDCAs (uCDCA, gCDCA, and tCDCA),¹⁷ and DCAs (uDCA, gDCA, and tDCA),¹⁶ in the relevant compartments. All reaction rates are described using first-order rate equations (except for CA and CDCA syntheses, which are described using zero-order equations); some of the reactions (intestinal motility and colonic

motility, gallbladder emptying) are modulated by meal ingestion (constant rates of these processes are multiplied by step-wise, time-dependent functions). All model parameters can be divided into 2 main groups: physiological parameters (organ compartments, blood flows, and intestinal motility), which correspond to physiological properties of an organism and are the same for all BAs; and BA-specific parameters, which may differ for individual BAs and represent synthesis rates as well as passive and active transport across biological membranes (absorption from the gastrointestinal tract to the portal circulation, hepatic uptake).

The following modifications were applied to the original models. First, the present model considers a simultaneous description of all key BAs and their conjugates (uCA, uCDCA, uDCA, gCA, gCDCA, gDCA, tCA, tCDCA, and tDCA). Second, meal-induced changes in the portal circulation and ileal BA deconjugation are introduced. Third, regulation of BA synthesis (mirrored by C4 levels) by transintestinal BA flux, as mediated by FGF-19, and by transhepatic BA flux, was introduced. Fourth, although negligible in healthy subjects, colonic absorption of primary BAs (CA and CDCA) was considered because it may become important in specific pathologic conditions (eg, ileal resection). Fifth, given these modifications, some model parameters were re-estimated using additional experimental data.

Model Limitations

To provide a mechanistic description of BA distribution and still meet model identifiability criteria, several assumptions were made.

First, hepatocellular and cholangiocellular BA transport is mediated by multiple systems (eg, NTCP, OATPs).⁴¹ Differentiation of these pathways is challenging and would require additional experimental data (transporter expression, affinities, and so forth); we did not consider such differentiation in the present model. BA secretion from the liver to the biliary tract is assumed to be similar across all BAs, as assumed in the original models, based on similarities in individual BA levels in liver tissue and bile. Second, BA competition for transporters is not taken into account in the model. Third, relative contributions of the BA-mediated hepatic FXR vs FGF-19-mediated Fibroblast growth factor receptor 4 (FGFR4) effect on BA synthesis were not differentiated in the model because of insufficient experimental evidence. Fourth, modulation of BA transporter expression by FXR was not considered in the model owing to insufficient clinical data that would allow for an accurate quantification of this mechanism. Based on experiments with CDCA administration, hepatic CA uptake can be inhibited moderately by FXR activation ($79\% \pm 5\%$ vs $74\% \pm 4\%$, for untreated vs CDCA-fed patients).⁴⁸ Fifth, some processes might be left out of scope in the healthy state but may become important under specific pathologic conditions (eg, activation of the cholehepatic shunt, renal BA clearance, hepatic FGF-19 synthesis under cholestatic conditions). Sixth, despite jejunal permeability of unconjugated BAs being shown to be much higher vs conjugated ones,^{27,49} unconjugated BA absorption from the jejunum was not

considered in the model because only conjugated BAs are presented in the upper intestine.²⁵ This rate, however, can be considered to accurately reproduce the exogenous intake of unconjugated BAs, followed by their appearance in the small intestine.

Model Structure

The final model is represented by a system of 74 ODEs and includes 117 reaction rates. The set of ODEs reflecting the anatomic structure of the model is presented later, with further specifications of individual BA distributions, followed by a description of reaction rates.

ODE system. The level of unconjugated BAs in the liver is dependent on hepatic uptake from the sinusoidal space and de novo synthesis of primary BAs (CA and CDCA). In the liver, BAs undergo conjugation with taurine or glycine. Hence, individual unconjugated BA (uBA) amounts in the liver may be described by [equation 1](#), as follows:

$$\frac{duBA_{LIV}}{dt} = (V_{syn} + V_{hupt}) - (V_{ref} + V_{conj}) \quad (1)$$

Where $uBA_{LIV} = uCA, uCDCA$ or $uDCA$ represent amounts in the liver, V_{syn} is the hepatic BA (uCA or $uCDCA$) synthesis rate, V_{ref} and V_{hupt} are rates of hepatic BA ($uCA, uCDCA$, or $uDCA$) uptake and BA reflux from the liver, and V_{conj} is the rate of BA ($uCA, uCDCA$, or $uDCA$) conjugation with glycine and taurine.

BAs conjugated in the liver, as well as those conjugated BAs (cBA) absorbed from the sinusoidal space, can be returned to the sinusoidal space or excreted to the bile ducts ([equation 2](#)), as follows:

$$\frac{dcBA_{LIV}}{dt} = (V_{conj} + V_{hupt}) - (V_{ref} + V_{sec}) \quad (2)$$

Where $cBA_{LIV} = tCA$, and $tCDCA, tDCA, gCA, gCDCA$, or $gDCA$ represent amounts in the liver. V_{sec} is the BA ($tCA, tCDCA, tDCA, gCA, gCDCA$, or $gDCA$) transport from the liver to the bile ducts.

Only cBAs are present in the biliary tract. cBA flux from the liver is partitioned between the gallbladder and the common duct ([equation 3](#)), as follows:

$$\frac{dcBA_{BD}}{dt} = V_{sec} - (V_{fill_{GB}} + V_{fastsec}) \quad (3)$$

Where $cBA_{BD} = tCA; tCDCA, tDCA, gCA, gCDCA$, or $gDCA$ represent amounts in the bile ducts; $V_{fill_{GB}}$ and $V_{fastsec}$ are rates of gallbladder filling and fasting BA ($tCA, tCDCA, tDCA, gCA, gCDCA$, or $gDCA$) secretion.

Gallbladder emptying into the small intestine occurs in response to meal ingestion ([equation 4](#)), as follows:

$$\frac{dcBA_{GB}}{dt} = V_{fill_{GB}} - V_{empt_{GB}} \quad (4)$$

Where $cBA_{GB} = tCA; tCDCA, tDCA, gCA, gCDCA$, or $gDCA$ represent amounts in the gallbladder; and $V_{empt_{GB}}$ is the rate of gallbladder emptying.

Some fraction of $gCDCA$ and $gDCA$ is absorbed in the upper intestine, whereas most BAs transit to the ileum

(equation 5), as follows:

$$\frac{dcBA_{U\text{INT}}}{dt} = V_{\text{empt}_{\text{GB}}} - (V_{\text{abs}_{\text{SUI\text{NT}}} + V_{\text{tr}_{\text{INTINT}}}) \quad (5)$$

Where $cBA_{\text{U\text{INT}}} = t\text{CA}$; $t\text{CDCA}$, $t\text{DCA}$, $g\text{CA}$, $g\text{CDCA}$, or $g\text{DCA}$ represent amounts in the duodenojejenum; $V_{\text{abs}_{\text{SUI\text{NT}}}}$ is the rate of jejunal BA ($g\text{CDCA}$ or $g\text{DCA}$) absorption; and $V_{\text{tr}_{\text{INTINT}}}$ is the rate of intestinal BA ($t\text{CA}$, $t\text{CDCA}$, $t\text{DCA}$, $g\text{CA}$, $g\text{CDCA}$, or $g\text{DCA}$) transit.

In the lower intestine, BAs undergo absorption or deconjugation with a minor part escaping to the colon (equations 6 and 7), as follows:

$$\frac{dcBA_{\text{LINT}}}{dt} = V_{\text{tr}_{\text{INTINT}}} - (V_{\text{tr}_{\text{INTCOL}}} + V_{\text{dcj}_{\text{INT}}} + V_{\text{abs}_{\text{LINT}}}) \quad (6)$$

$$\frac{duBA_{\text{LINT}}}{dt} = V_{\text{dcj}_{\text{INT}}} - (V_{\text{tr}_{\text{INTCOL}}} + V_{\text{abs}_{\text{LINT}}}) \quad (7)$$

Where $cBA_{\text{LINT}} = t\text{CA}$, $t\text{CDCA}$, $t\text{DCA}$, $g\text{CA}$, $g\text{CDCA}$, or $g\text{DCA}$ and $uBA_{\text{LINT}} = u\text{CA}$, $u\text{CDCA}$, $u\text{DCA}$ represent amounts in the ileum; $V_{\text{tr}_{\text{INTCOL}}}$ and $V_{\text{dcj}_{\text{INT}}}$ are the rates of intestinal BA transit (all BAs) and deconjugation of $c\text{BA}$ in the lower intestine.

The colon is the main site of BA deconjugation (equation 8), as follows:

$$\frac{dcBA_{\text{COL}}}{dt} = V_{\text{tr}_{\text{INTCOL}}} - (V_{\text{dcj}_{\text{COL}}} + V_{\text{ex}}) \quad (8)$$

Where $cBA_{\text{COL}} = t\text{CA}$; $t\text{CDCA}$, $t\text{DCA}$, $g\text{CA}$, $g\text{CDCA}$, or $g\text{DCA}$ represent amounts in the colon; and $V_{\text{dcj}_{\text{COL}}}$ is the rate of $c\text{BA}$ ($t\text{CA}$, $t\text{CDCA}$, $t\text{DCA}$, $g\text{CA}$, $g\text{CDCA}$, or $g\text{DCA}$) deconjugation in the colon.

Primary uBAs ($u\text{CA}$, $u\text{CDCA}$) can be transformed by colon microbiota: 7α -dehydroxylation of $u\text{CA}$ results in the formation of $u\text{DCA}$, which can be absorbed or excreted with feces; 7α -dehydroxylation of $u\text{CDCA}$ results in formation of secondary BAs, which are not considered in the model. In the original model, $u\text{DCA}$ was assumed to be synthesized in insoluble form and can be absorbed only after solubilization, both insoluble and soluble DCA forms undergo fecal excretion¹⁶ (equations 9–11), as follows:

$$\frac{duBA_{\text{COL}}}{dt} = (V_{\text{tr}_{\text{INTCOL}}} + V_{\text{dcj}_{\text{COL}}}) - (V_{\text{dhx}} + V_{\text{ex}} + V_{\text{abs}_{\text{COL}}}) \quad (9)$$

$$\frac{du\text{DCA}_{\text{insol}_{\text{COL}}}}{dt} = (V_{\text{dhx}}) - (V_{\text{ex}} + V_{\text{sol}}) \quad (10)$$

$$\frac{du\text{DCA}_{\text{COL}}}{dt} = (V_{\text{tr}_{\text{INTCOL}}} + V_{\text{dcj}_{\text{COL}}} + V_{\text{sol}}) - (V_{\text{ex}} + V_{\text{abs}_{\text{COL}}}) \quad (11)$$

Where $uBA_{\text{COL}} = u\text{CA}$; $u\text{CDCA}$ represent amounts in colonic space; V_{dhx} is the rate of primary uBA ($u\text{CA}$, $u\text{CDCA}$)

dehydroxylation; V_{ex} is the rate of fecal uBA excretion ($u\text{CA}$, $u\text{CDCA}$, $u\text{DCA}$); V_{sol} is the rate of $u\text{DCA}$ solubilization; and $V_{\text{abs}_{\text{COL}}}$ is the rate of colonic soluble $u\text{DCA}$ absorption.

Once absorbed from the upper and lower intestine and colon, BAs enter the portal vein. Further BA distribution within the systemic and portal circulations is determined by plasma fluxes; the corresponding rates and parameters all were the same for all BAs considered in the model. From the portal vein, BAs enter the sinusoidal space where they can be extracted by the liver. Parts of BAs enter the systemic circulation via the hepatic vein, where they may return to the portal circulation via mesenteric blood flow. BA distribution between the portal and systemic circulations can be described by the following set of ODEs (equations 12–14), as follows:

$$\frac{dBA_{\text{PV}}}{dt} = (V_{\text{tr}_{\text{MA}}} + V_{\text{abs}_{\text{SUI\text{NT}}} + V_{\text{abs}_{\text{LINT}}} + V_{\text{abs}_{\text{COL}}}) - V_{\text{tr}_{\text{PV}}} \quad (12)$$

$$\frac{dBA_{\text{SIN}}}{dt} = V_{\text{tr}_{\text{PV}}} - (V_{\text{hupt}} + V_{\text{tr}_{\text{HA}}}) \quad (13)$$

$$\frac{dBA_{\text{SYS}}}{dt} = V_{\text{tr}_{\text{HA}}} - V_{\text{tr}_{\text{HV}}} - V_{\text{tr}_{\text{MA}}} \quad (14)$$

Where BA_{PV} , BA_{SIN} , and $BA_{\text{SYS}} = u\text{CA}$; $u\text{CDCA}$, $u\text{DCA}$, $t\text{CA}$, $t\text{CDCA}$, $t\text{DCA}$, $g\text{CA}$, $g\text{CDCA}$, or $g\text{DCA}$ represent amounts in the portal vein, sinusoidal space, and systemic circulation, respectively; $V_{\text{tr}_{\text{MA}}}$, $V_{\text{tr}_{\text{PV}}}$, $V_{\text{tr}_{\text{HA}}}$, and $V_{\text{tr}_{\text{PV}}}$ are the corresponding BA fluxes within the mesenteric artery, portal vein, hepatic artery, and hepatic vein.

Reaction rates. Reaction rates are described as zero- or first-order rate equations. Because some processes (gallbladder emptying, gastric motility, portal circulation, and deconjugation) are affected by meal ingestion, rate constants for these reactions are multiplied by time-dependent functions reflecting food intake dynamics.

Synthesis of primary BAs ($u\text{CA}$ and $u\text{CDCA}$) in the liver is described using zero-order rate equations. $u\text{CA}$ synthesis is controlled by FXR (equations 15 and 16), as follows:

$$V_{\text{syn}_{\text{CA}}} = k_{\text{syn}_{\text{CA}}} \cdot \text{FXR}_{\text{syn}} \quad (15)$$

$$V_{\text{syn}_{\text{CDCA}}} = k_{\text{syn}_{\text{CDCA}}} \quad (16)$$

Where $k_{\text{syn}_{\text{CA}}}$ and $k_{\text{syn}_{\text{CDCA}}}$ are rate coefficients for $u\text{CA}$ and $u\text{CDCA}$ synthesis, and FXR_{syn} is a function describing the negative effect of FXR activation on CA synthesis.

BA conjugation with glycine and taurine in the liver is similar across uBAs (equations 17 and 18), as follows:

$$V_{\text{conj}_{\text{tau}}} = k_{\text{conj}} \cdot f_{\text{tau}}^{\text{conj}} \cdot uBA_{\text{LIV}} \quad (17)$$

$$V_{\text{conj}_{\text{gly}}} = k_{\text{conj}} \cdot (1 - f_{\text{tau}}^{\text{conj}}) \cdot uBA_{\text{LIV}} \quad (18)$$

Where $uBA_{LIV} = uCA$; $uCDCA$ or $uDCA$ represent amounts in the liver; k_{conj} is a rate constant for BA conjugation; and fr_{τ}^{conj} is a fraction of BAs conjugated with taurine.

The flux of BA from the liver to the biliary tract includes transport across the canalicular membrane, mediated mainly via bile salt export pump transporter and cholangiocellular transport mediated via ASBT.⁴¹ Based on similar CA, CDCA, and DCA proportions in the liver tissue and duodenal bile, the excretion of individual BAs to the biliary tract was assumed to be similar^{23,40} (equation 19), as follows:

$$V_{sec} = k_{secLIV} \cdot cBA_{LIV} \quad (19)$$

Where $cBA_{LIV} = tCA$; $tCDCA$, $tDCA$, gCA , $gCDCA$, or $gDCA$ represent amounts in the liver, and k_{secLIV} are rate constants for BA transport from the liver to the biliary tract.

Parameters for BA distribution within the biliary tract are the same for all BAs considered in this model. Only cBAs are presented here (equations 20–22), as follows:

$$V_{fill_{GB}} = \frac{Q_{sec}}{BD} \cdot fr_{GB}^{fill} \cdot cBA_{BD} \quad (20)$$

$$V_{fastsec} = \frac{Q_{sec}}{BD} \cdot (1 - fr_{GB}^{fill}) \cdot cBA_{BD} \quad (21)$$

$$V_{empt_{GB}} = k_{empt_{GB}} \cdot cBA_{GB} \cdot tf_{GB}^{empt} \quad (22)$$

Where cBA_{BD} and $cBA_{GB} = tCA$; $tCDCA$, $tDCA$, gCA , $gCDCA$, or $gDCA$ represent amounts in the bile duct and gallbladder, respectively; BD is the volume of the bile duct space; Q_{ex} is the total conjugated BA flow from the liver; Q_{sec} is the total conjugated BA flow from the BD; fr_{GB}^{fill} is a conjugated BA fraction that goes to the gallbladder; and tf_{GB}^{empt} is a time-dependent function for gallbladder emptying.

The flux of BA along the intestine is determined by gastrointestinal motility, which itself is affected by meal consumption (equations 23 and 24), as follows:

$$V_{tr_{INTINT}} = k_{tr_{INTINT}} \cdot tf_{GUT}^{tr} \cdot cBA_{UINT} \quad (23)$$

$$V_{tr_{INTCOL}} = k_{tr_{INTCOL}} \cdot tf_{GUT}^{tr} \cdot BA_{LINT} \quad (24)$$

Where $cBA_{UINT} = tCA$; $tCDCA$, $tDCA$, gCA , $gCDCA$, or $gDCA$ represent amounts in the upper intestine; $BA_{LINT} = uCA$; $uCDCA$, $uDCA$, tCA , $tCDCA$, $tDCA$, gCA , $gCDCA$, or $gDCA$ represent amounts in the lower intestine; and $k_{tr_{INTINT}}$ and $k_{tr_{INTCOL}}$ are transport constants for intestinal and colonic BA transit, affected by a time-dependent function tf_{GUT}^{tr} .

Ileal deconjugation of glycine-conjugated BAs (gBAs) is faster than that of taurine-conjugated BAs (tBAs) and is modulated by a time-dependent function tf_{INT}^{mbt} (equation 25), as follows:

$$V_{dcj_{INT}} = k_{dcj_{LINT}} \cdot cBA_{LINT} \cdot tf_{INT}^{mbt} \quad (25)$$

Where $cBA_{LINT} = tCA$; $tCDCA$, $tDCA$, gCA , $gCDCA$, or $gDCA$

represent amounts in the ileum; and $k_{dcj_{LINT}}$ is a rate constant for BA deconjugation in the lower intestine.

BA deconjugation in the colon is similar for all BAs, as described in the original published models (equation 26), as follows:

$$V_{dcj_{COL}} = k_{dcj_{COL}} \cdot cBA_{COL} \quad (26)$$

Where $cBA_{col} = tCA$; $tCDCA$, $tDCA$, gCA , $gCDCA$, or $gDCA$ represent amounts in the colon; and $k_{dcj_{COL}}$ is a rate constant for BA deconjugation in the lower intestine, similar for all BAs.

Dehydroxylation represents the main route of primary BA elimination and is different across uCA and $uDCA$ (equation 27), as follows:

$$V_{dhx} = k_{dhx} \cdot uBA_{col} \quad (27)$$

Where $uBA_{col} = uCA$; $uCDCA$ represent amounts in colon; and k_{dhx} is a rate constant for BA dehydroxylation (uCA , $uCDCA$).

Synthesized DCA then undergoes solubilization (equation 28), as follows:

$$V_{sol} = k_{sol} \cdot uDCA_{insol_{COL}} \quad (28)$$

Where k_{sol} is a rate constant for DCA solubilization.

Few primary BAs are present in feces because most of them are reabsorbed or dehydroxylated in the colon. Hence, we only considered fecal excretion of $uDCA$ in the model (equation 29), as follows:

$$V_{ex} = k_{ex} \cdot uBA_{COL} \quad (29)$$

Where $uBA_{COL} = uCA$; $uCDCA$ or $uDCA$ represent amounts in the colon; and k_{ex} is a rate coefficient.

BA absorption from the gastrointestinal tract differs among individual BAs. In the upper intestine, $gCDCA$ and $gDCA$ are predominantly absorbed.¹⁵ BA absorption in the lower intestine differs among individual BAs and is determined by respective affinities to ASBT receptors and passive permeability. Predominantly $uDCA$ is absorbed in the colon in the healthy state, whereas $uCDCA$ and $uDCA$ absorption is possible under pathologic conditions (equations 30–32), as follows:

$$V_{abs_{UINT}} = k_{abs_{UINT}} \cdot cBA_{UINT} \quad (30)$$

$$V_{abs_{LINT}} = k_{abs_{LINT}} \cdot BA_{LINT} \quad (31)$$

$$V_{abs_{COL}} = k_{abs_{COL}} \cdot uBA_{COL} \quad (32)$$

Where $cBA_{UINT} = gCDCA$; $gDCA$ represent amounts in the upper intestine; and $k_{abs_{UINT}}$ is a rate coefficient, similar for $gCDCA$ and $gDCA$. $BA_{LINT} = uCA$; $uCDCA$, $uDCA$, tCA , $tCDCA$, $tDCA$, gCA , $gCDCA$, or $gDCA$ represent amounts in the ileum; $k_{abs_{LINT}}$ is a rate coefficient, different across BAs. $uBA_{col} = uCA$; $uCDCA$, and $uDCA$ represent amounts in the colonic space; and $k_{abs_{COL}}$ is a rate coefficient, different across BAs.

BA fluxes within the portal and systemic circulation are determined by rates of blood fluxes divided by organ volumes (equations 33–36), as follows:

$$V_{tr_{MA}} = \frac{Q_{MA}}{SYS} \cdot BA_{SYS} \cdot tf_{CIRC}^{tr} \quad (33)$$

$$V_{tr_{HA}} = \frac{Q_{HA}}{HA} \cdot BA_{HA} \cdot tf_{CIRC}^{tr} \quad (34)$$

$$V_{tr_{HV}} = \frac{Q_{HV}}{HV} \cdot BA_{HV} \cdot tf_{CIRC}^{tr} \quad (35)$$

$$V_{tr_{PV}} = \frac{Q_{PV}}{PV} \cdot BA_{PV} \cdot tf_{CIRC}^{tr} \quad (36)$$

Where BA_{SYS} , BA_{HA} , BA_{HV} , and BA_{MA} are uCA, uCDCA, uDCA, tCA; tCDCA, tDCA, gCA, gCDCA, or gDCA represent amounts in the systemic, hepatic artery and vein, and mesenteric artery, respectively; MA, HA, HV, and PV, Q_{MA} , Q_{HA} , Q_{HV} , and Q_{PV} are volumes of the mesenteric artery, hepatic artery, hepatic vein, and portal vein and corresponding blood fluxes, multiplied by a time-dependent function tf_{CIRC}^{tr} .

BA exchange between liver tissue and the sinusoidal space is bidirectional. Hepatic BA uptake is performed via OATPs and NTCP transporters, whereas reflux from the liver to the sinusoidal space is mediated via organic solute transporters and multidrug-resistance protein 3, 4 (MRP3, 4) transporters. BA reflux from the liver was assumed to be negligible in the healthy state (equations 37 and 38), as follows:

$$V_{hupt} = khupt \cdot BA_{SIN} \quad (37)$$

$$V_{ref} = kref \cdot BA_{LIV} \quad (38)$$

Where $BA_{LIV} = uCA$; uCDCA, uDCA, tCA, tCDCA, tDCA, gCA, gCDCA, or gDCA represent amounts in the liver; and kref is a rate constant for BA reflux from the liver to the sinusoidal space.

FXR-mediated BA autoregulation. The regulatory feedbacks proposed in the model are described using explicit functions. A competitive binding equation was used to link BA dynamics with FXR activation (equation 39), as follows:

$$FXRa = Fmax_{FXR}^{BA} \cdot \sum \left(\frac{BA_{LINT}}{EC50_{ba}^{fxr} \cdot LINT} \right) / \left(\sum \left(\frac{BA_{LINT}}{EC50_{FXR}^{BA} \cdot LINT} \right) + 1 \right) \quad (39)$$

Where $BA_{LINT} = (tCA, tCDCA, tDCA, gCA, gCDCA \text{ or } gDCA, uCA, uCDCA, uDCA)$; FXRa represents normalized (to fasting FXR in healthy subjects) FXR activation by BAs; Kd_{eff} represents concentrations of individual BAs in the lower intestine, associated with a 50% FXR activation; $Vmax_{ba}^{fxr}$ is

the maximal FXR activation by BAs; and the median effective concentration $(EC50)_{ba}^{fxr}$ is an effective BA parameter, multiplied by a scaling factor, different across individual BAs.

A delay between intestinal BAs and FXR activation, tracked by plasma FGF-19, was assumed based on experimental evidence from Al-Khaifi et al.⁹ To describe the delay, an additional ODE was introduced (equation 40), as follows:

$$\frac{dFGF-19}{dt} = kdel \cdot (FXRa - FGF - 19) \quad (40)$$

Where FGF-19 represents the normalized plasma FGF-19 concentration, equal to 1 in healthy subjects after overnight fasting, and kdel represents the delay between FXR activation and systemic FGF-19 levels.

The relationship between systemic FGF-19 and CYP7A1 activity was described using the following exponential-like equation, implying no FGF-19 is present in the case of complete absence of BAs and is equal to 1 in healthy subjects after overnight fasting (equation 41), as follows:

$$C4 = \exp \left(a_{fgf19}^{ba} \cdot (1 - FGF - 19) \right) \quad (41)$$

Where a_{fgf19}^{ba} is a parameter describing the FGF-19 effect on BA synthesis reflected by C4 changes in the systemic circulation.

Equation 41 allows for a sustained daily C4 variation in a (0, 1) range. This function should be modified to ensure daily BA synthesis equal to CA synthesis constant $ksyn_{CA}$, based on daily CA production. To do so, the area under daily C4 dynamics should be equal to 0, which can be achieved by using equation 42, as follows:

$$FXR_{syn} = C4 + b_{fgf19}^{ba} \quad (42)$$

Where b_{fgf19}^{ba} is a parameter that ensures $AUC_{0-24}(C4) = 0$. **Time-dependent functions.** Time-dependent functions are conditional statements controlling step-wise parameter changes within specified time intervals.

Emptying of the gallbladder occurs within 1.5 hours after meal ingestion (equation 43), as follows:

$$\text{If } (time_{meal} < t < time_{meal} + GBempt_{dur}) \text{ then } \{tf_{GB}^{empt} = 1\} \text{ else } \{tf_{GB}^{empt} = 0\} \quad (43)$$

Where $time_{meal}$ is the time of meal ingestion, and $GBempt_{dur}$ is the duration of gallbladder contraction.

Gastric motility and portal circulation are activated in the postprandial period, whereas gut microbiota is suppressed. These processes are assumed to change simultaneously (equation 44), as follows:

$$\text{If } (time_{meal} < t < time_{meal} + DIST_{dur}) \text{ then } \{tf_{CIRC}^{tr} = b\} \{tf_{INT}^{tr} = c\} \{tf_{INT}^{mbt} = 0\} \text{ else } \{tf_{CIRC}^{tr} = 1\} \{tf_{INT}^{tr} = 1\} \{tf_{INT}^{mbt} = 1\} \quad (44)$$

Where $DIST_{dur}$ is the duration of meal effect on gastric motility and portal circulation, and b and c are coefficients describing increases in rate constants for these processes.

Model Verification Against Experimental Data

The model includes 59 parameters, 23 of which are related to basic physiology (organ volumes and physiological fluxes), 32 are BA-specific (synthesis, transmembrane transport, biotransformation), and 4 are FXR-related. Physiological parameter values are common for all BAs and consistent with values used in previous publications (Table 1).^{15,24} BA-specific parameter values differed across various BAs (Table 2). These parameters were as follows: (1) taken directly from the literature, (2) fixed based on observations from specific experiments (eg, in vitro studies), and (3) estimated using experimental measurements. Parameter estimation was performed based on a maximum likelihood-based method using a trust-region optimizer.

Publicly available study-level data were used in the current work (Table 3), which included the following: (1) measurements of individual BAs and their conjugates in peripheral and portal blood, liver biopsy specimens, biliary, jejunal, and ileal bile, and in feces from healthy subjects^{9,21–25,39,40,50–54}; (2) measurements of systemic C4 (a marker of BA synthesis by CYP7A1) and of FGF-19 (a marker of intestinal FXR activation) obtained from healthy subjects and patients with ileal resections^{5,9}; and (3)

intestinal and colonic permeability data for individual BAs obtained from perfusion studies.^{27,28} In addition, in vitro data were used to estimate the relative affinities of individual BAs for FXR.²⁹

A detailed description of parameter calculations is reported later.

Parameters for hepatic BA uptake were calculated previously and reported by Al-Khaifi et al.⁹ Primary BA (CDCA and CA) synthesis constants were calculated from Pattni and Walters.³⁶ BA absorption in the upper intestine was determined previously based on CA, CDCA, and DCA fractions in the upper and lower intestine⁴⁰ and used in the Hofmann et al models.¹⁶ Relative ileal wall permeabilities for individual BAs were set based on perfusion studies by Krag and Phillips.²⁷ Absorption of conjugated CDCA and DCA (gCDCA, tCDCA, gDCA, tDCA) is 3-fold lower vs unconjugated CDCA and DCA (uCDCA and uDCA). Absorption of tCA is approximately 20% lower than that of uCDCA and similar to uCA. ($k_{\text{LINT}}^{\text{gCA}} : k_{\text{LINT}}^{\text{gCDCA}} : k_{\text{LINT}}^{\text{gDCA}} : k_{\text{LINT}}^{\text{tCA}} : k_{\text{LINT}}^{\text{tCDCA}} : k_{\text{LINT}}^{\text{tDCA}} : k_{\text{LINT}}^{\text{uCA}} : k_{\text{LINT}}^{\text{uCDCA}} : k_{\text{LINT}}^{\text{uDCA}} = 1:0.4:0.4:1:0.4:0.4:1:1.2:1.2$). Relative colonic wall permeabilities for individual BAs were set based on perfusion studies by Mekhjian et al²⁸ ($k_{\text{COL}}^{\text{uCA}} : k_{\text{COL}}^{\text{uCDCA}} : k_{\text{COL}}^{\text{uDCA}} = 1:10:6.5$). Comparison of ileal and colonic BA absorptions from these

Table 1. System-Specific (Physiological and FXR-Related) Parameters

Parameter	Description	Value	Dimension	Estimation
Organ volumes				
PL	Systemic circulation	2.5	L	Taken ¹⁵
PV	Portal circulation	0.45	L	Taken ¹⁵
LIV	Liver	0.9	L	Taken ¹⁵
BD	Bile duct	0.045	L	Taken ¹⁵
GB	Gallbladder	0.03	L	Taken ¹⁵
UINT	Upper intestine	0.2	L	Taken ¹⁵
LINT	Lower Intestine	0.1	L	Taken ¹⁵
COL	Colon	0.3	L	Taken ¹⁵
SIN	Sinusoidal space	0.2	L	Taken ¹⁵
Fluxes				
Q _{MA}	Mesenteric artery plasma flow	600	mL/min	Taken ²⁴
Q _{PV}	Portal vein plasma flow	600	mL/min	Taken ²⁴
Q _{HA}	Hepatic artery plasma flow	200	mL/min	Taken ²⁴
Q _{HV}	Hepatic vein plasma flow	800	mL/min	Taken ²⁴
Q _{seq}	Biliary secretion	0.45	mL/min	Taken ¹⁷
f _{GB} ^{fill}	BA fraction to the GB	0.3	–	Calculated ¹⁷
f _{tau} ^{conj}	BA fraction being conjugated with taurine	0.25	–	Calculated ¹⁷
kempt _{GB}	Gallbladder emptying	1.2	1/h	Taken ¹⁷
ktr _{intint}	Gastric motility fasting	0.18	1/h	Taken ¹⁷
ktr _{intcol}	Gastric motility fasting	0.12	1/h	Taken ¹⁷
kex	Colonic motility	0.07	1/h	Calculated ⁶
FXR-related parameters				
kdel	Delay between FXR activation and FGF-19 synthesis	0.4	1/h	Fixed based on ⁹
Fmax _{FXR} ^{BA}	Maximum FXR activation by BAs	2	–	Fixed based on ³⁴
EC50 _{FXR}	BA amount inducing 50% FXR activation	55	umol	Estimated ⁹
b _{Igf19} ^{ba}	Correction factor for FGF-19 effect on BA synthesis	0.2	–	Fixed to ensure daily area under C4 curve = 1

Table 2. BA-Specific Parameters

Parameter	Process	uCA	uCDCA	uDCA	tCA	tCDCA	tDCA	gCA	gCDCA	gDCA	Dimension	Estimation
ksyn	Synthesis	27	18	–	–	–	–	–	–	–	umol/h	Taken ^{21,36}
ksol	Solubilization	–	–	0.04	–	–	–	–	–	–	1/h	Estimated, pooled data
kconj	Conjugation	4.8	4.8	4.8	–	–	–	–	–	–	1/h	Taken ¹⁷
ksec _{LIV}	Biliary secretion	–	–	–	12	12	12	12	12	12	1/h	Taken ¹⁵
fdcj _{IL}	Scaling factor for tBA and gBA deconjugation	–	–	–	1	1	1	4	4	4	–	Set based on previous estimations ¹⁷
kdcj _{COL}	Colonic deconjugation	–	–	–	5	5	5	5	5	5	1/h	Selected based on sensitivity analysis
kdhx	Dehydroxylation	0.33	0.6285	–	–	–	–	–	–	–	1/h	Estimated, pooled data
kex	Fecal excretion	–	–	0.07	–	–	–	–	–	–	1/h	Calculated from colonic transit time ⁶
kabs _{UINT}	UINT absorption	–	–	–	–	–	–	–	0.09	0.09	1/h	Taken ¹⁵
fabs _{LINT}	Scaling factor for LINT absorption	2.5	3	3	2.5	1	1	7.5	1	1	–	Set based on perfusion studies ²⁷
fabs _{COL}	Scaling factor for COL absorption	0.02	0.2	0.13	–	–	–	–	–	–	–	Set based on perfusion studies ²⁸
khupt	Hepatic uptake	724	243	190	2016	848	720	2016	848	720	1/h	Taken ⁹
fFXR	Scaling factor for EC50 _{BA} ^{FXR}	–	4	8	5	1.7	1.7	5	1.7	1.7	–	Set based on in vitro data ²⁹

COL, colon; gBA, glycine-conjugated BAs; LINT, lower intestine; tBA, taurine-conjugated BAs; UINT, upper intestine.

perfusion studies showed that colonic permeability for uCDCA is 15 times lower vs ileal permeability (Figure 8).

Because relative intestinal and colonic permeabilities for individual BAs were fixed in the model, the only parameter reflecting overall BA absorption was estimated based on pooled data from Table 3. The absorption rate constants for individual BAs then were calculated using equations 45 and 46, as follows:

$$kabs_{LINT} = kabs \cdot fabs_{LINT} \quad (45)$$

$$kabs_{COL} = kabs \cdot fabs_{COL} \quad (46)$$

Where $kabs_{LINT}$ and $kabs_{COL}$ are absorption constants for individual BAs in the lower intestine and the colon, respectively; $fabs_{LINT}$ and $fabs_{COL}$ are scaling factors that denote the aforementioned relative ileal and colonic permeabilities for individual BAs; and $kabs$ is an absorption constant, common to all individual BAs.

Relative individual BA potencies for FXR were set based on in vitro studies²⁹ (tCDCA:tDCA:tDCA:gDCA:tCA:gCA:CDCA:DCA = 1:1:0.58:0.58:0.2:0.2:0.25:0.125, respectively). FXR activation by uCA was assumed to be negligible based on experimental data.²⁹

The EC50s for FXR activation by individual BAs then were calculated using equation 47, as follows:

$$EC50_{FXR}^{BA} = fFXR / EC50_{FXR} \quad (47)$$

Where $EC50_{FXR}^{BA}$ are EC50s for individual BAs; $fFXR$ is a scaling factor that denotes the aforementioned relative BA potencies; and $EC50_{FXR}$ is a parameter common to all BAs.

Intestinal deconjugation of taurine conjugates was set 5 times lower compared with glycine conjugates based on the Hofmann et al^{15,16} models; the corresponding rate constants for individual BAs then were expressed using equation 48, as follows:

$$kdcj_{LINT}^{BA} = kdcj_{LINT} \cdot fdcj_{LINT} \quad (48)$$

Where $kdcj_{LINT}^{BA}$ are ileal deconjugation constants for individual BAs, $fdcj_{LINT}$ is a scaling factor that denotes the aforementioned relative BA deconjugation rates. Parameter $kdcj_{LINT}$ is common to all BAs and was estimated automatically using the pooled data from Table 3.

Colonic deconjugation was assumed to be similar for all BAs; colonic deconjugation in the Hofmann et al^{15,16} models was set as a constant to ensure complete colonic BA deconjugation. We updated the model with an approximately 3% conjugated BA fraction in the colon, in line with clinical data.²²

Table 3. Summary of Experimental Data Used

Reference	Tissue	Study population	Study design	Key information
9	Systemic circulation	8 HS	Standard meal 4 times/d	CA, CDCA, DCA, FGF-19, C4
24	Systemic and portal circulation	5 patients (CST)	Overnight fasting and postprandial measurements	CA, CDCA, DCA in PV, SYS
25	Small intestine	11 HS	Postprandial (jejunum, 30 min; lower intestine, <2 h)	uBA, cBA in UINT, LINT
23	Liver biopsy	8 HS	Overnight fasting	CA, CDCA, DCA in LIV
50	BD bile (surgical samples)	12 HS	Overnight fasting	TBA in BD
50	GB bile	8 HS	Overnight fasting	TBA in GB
21	Feces	16 HS	–	TBA in feces
52	Duodenal bile	11 HS	–	CA, CDCA, DCA in biliary tract
40	Intestinal aspirates (80, 180 cm from teeth)	3 HS	Meal intake, cholecystokinin IV injection	CA, CDCA, DCA in the intestine
53	Systemic circulation	24 HS	Overnight fasting	CA, CDCA, DCA in plasma
39	Feces	Review from published studies	–	CA, CDCA, DCA in feces
54	Portal vein	15 HS	Overnight fasting	uCA in portal blood
22	Feces	22 HS	–	uCA in feces
5	Systemic circulation	19 HS, 17 patients (BAM)	Overnight fasting	C4 and FGF-19
29	In vitro	–	–	BA potencies for FXR
27	Jejunum and ileum	4 HS	Jejunal and ileal perfusion	Intestinal permeability for CA, CDCA, DCA
28	Colon	47 HS	Colonic perfusion	Colonic permeability for CA, CDCA, DCA

BAM, bile acid malabsorption; BD, bile duct; CST, cholecystectomy; GB, gallbladder; HS, healthy subject; IV, intravenous; LINT, lower intestine; LIV, liver; PV, portal vein; SYS, systemic circulation; TBA, total BA; uBA, unconjugated BA; UINT, upper intestine.

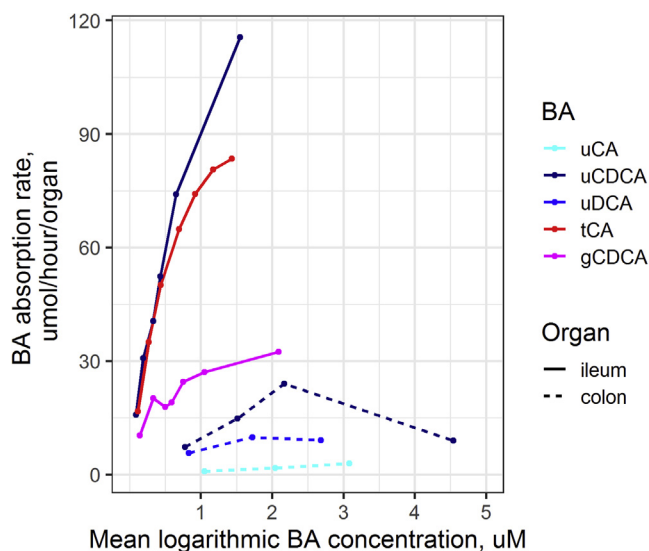


Figure 8. Comparison of ileal and colonic BA absorptions from published studies.^{27,28} In the original study²⁷ the BA absorption rate per 25 cm of the ileum was reported; in this Figure, it was recalculated for the total organ, assuming an ileal length of 220 cm.⁵⁶

Based on mass conservation law to maintain the pool of total primary BAs (CA and CDCA), daily primary BA production should be equal to their daily dehydroxylation. The latter represents a secondary BA synthesis route and should be equal to the fecal excretion of secondary BAs. CA and CDCA dehydroxylation constants and the constants for colonic DCA solubilization were estimated automatically using the pooled data from Table 3.

To quantify relationships between FGF-19 and BA synthesis (parameter $a_{\text{fgf19}}^{\text{ba}}$), experimental data for mean plasma FGF-19 and C4 levels collected from healthy subjects and patients with ileal resections were used. A

Table 4. Identifiability Analysis Results

Parameter	Estimated value	95% CI	Dimension
kabs	2.4060	2.3910–2.4210	1/h
kdh _{XCA}	0.3309	0.3276–0.3342	umol/h
ksol	0.0410	0.0405–0.0416	1/h
kdh _{XCDCA}	0.6285	0.6220–0.6351	1/h
kdcj _{LINT}	0.1373	0.1346–0.1400	1/h

delay in the BA effect on FXR was set to obtain a realistic delay of approximately 1.5 hours between BAs and FGF-19, based on previous estimates.⁹ A maximal BA effect on FXR was assumed, based on the average FGF-19 increase observed under CDCA feeding.³⁴ Parameter $EC50_{FXR}$, which describes the overall capacity of transintestinal BA flux in activating ileal FXR, was estimated to ensure a fasting FGF-19 level of 1 after overnight fasting in healthy subjects.

Identifiability Analysis, Model Diagnostics, and Validation

In total, 5 model parameters were estimated (Table 4); CIs for the parameter estimates were determined via the Fisher Information Matrix. Point-wise finite sample CIs were calculated through likelihood profiling. A summary of the identifiability analysis is reported in Table 4. CIs range within $\pm 5\%$ from the estimated values, ensuring adequate precision in parameter estimation (ie, the model is identifiable).

A multistart parameter estimation procedure, based on 100 repeats of the procedure from randomly

generated, physiologically plausible, initial parameter guesses, was performed to test whether the parameter optimization algorithm reached a global optimum in likelihood estimation.

To evaluate model appropriateness for reproduction of various pathologic states, validation against independent publicly available experimental observations from subjects with various EHC perturbations and abnormalities was performed. Given significant between-subject variability in the daily dynamics of the considered components (eg, individual BA fractions, C4, and FGF-19) as well as various pathologic states and interventions, model simulations were compared against corresponding data within expected physiological response ranges. Validation results are summarized in Table 5.

Software

Model development, calibration, and analyses were performed using the IQR toolbox (IntiQuan, Basel, Switzerland), based on R software version 3.4.1 (Vienna, Austria). Visualizations of model simulations were performed in R version 3.4.1, using the ggplot2 2.1.0 package.

Table 5. Model Validation Summary

Perturbation	Experimental observations	Simulation design	Simulation result	Comments
Food consumption	Total, conjugated BAs \uparrow , FGF-19 \uparrow , C4 \downarrow in the systemic plasma ⁹	Default parameter values	~ 2 -fold total BA \uparrow , driven by conjugated BAs, $\sim 35\%$ FGF-19 \uparrow and 70% C4 \downarrow in systemic plasma (Figure 3)	Gallbladder emptying depends on food fat content ¹⁸ ; hence, parameter $k_{empt_{GB}}$ can be changed to reflect different food types
Fasting (short term)	Total BAs and FGF-19 \downarrow , C4 \uparrow in the systemic plasma ³⁴	Time-dependent functions are fixed on fasting values: $tf_{GB}^{empt} = 0$, $tf_{CIRC}^{tr} = 1$, $tf_{INT}^{tr} = 1$, $tf_{INT}^{inbt} = 1$	~ 2 -fold total BA \downarrow , 2.75-fold C4 \uparrow , and 60% FGF-19 \downarrow in systemic plasma (Figure 6)	Additional modifications are required to reproduce prolonged fasting (1) - parameter k_{syn} should be decreased to reflect BA synthesis reduction ⁵⁵ ; (2) rate $V_{fill_{GB}}$ should be modified to limit gallbladder filling
SIBO	Total and unconjugated BAs \uparrow in systemic plasma ⁵⁴	10-fold increase in parameter $kdcj_{LINT}$, from default value	~ 2.2 -fold total BAs \uparrow in systemic plasma (Figure 4)	Deconjugation and unconjugated BA absorption in the duodenojejunal compartment should be introduced to reflect severe SIBO
BA malabsorption (after ileostomy or cholestiramine treatment)	FGF-19 \downarrow and C4 \uparrow in systemic plasma, increased fecal BA loss ⁵	Parameter $fabs_{LINT}$ variation from default value to 0	Up to 25-fold total colonic BA \uparrow , up to 16-fold systemic C4 \uparrow (Figure 5)	Parameters $k_{tr_{intcol}}$, k_{excan} can be modified to reflect accelerated colonic motility in patients with BA-induced diarrhea ⁵
Antibiotic treatment	Secondary BAs \downarrow in systemic plasma ⁴³	10-fold decrease in parameter $kdcj_{COL}$, from default value	~ 7 -fold DCA fraction \downarrow (Figure 4)	–
Cholecystectomy	Preservation of meal-induced daily BA oscillations, CA and CDCA pool \downarrow ³³	Parameter fr_{GB}^{fill} was nullified, parameter $kdcj_{LINT}$ was changed for patients with SIBO/CST	Preservation of meal-induced BA-oscillations, no change in CA and CDCA fractions (Figure 7)	–

SIBO, small intestine bacterial overgrowth.

References

- Holm R, Müllertz A, Mu H. Bile salts and their importance for drug absorption. *Int J Pharm* 2013;453:44–55.
- Copple BL, Li T. Pharmacology of bile acid receptors: evolution of bile acids from simple detergents to complex signaling molecules. *Pharmacol Res* 2016;104:9–21.
- Sjöberg BG, Straniero S, Angelin B, Rudling M. Cholestyramine treatment of healthy humans rapidly induces transient hypertriglyceridemia when treatment is initiated. *Am J Physiol Endocrinol Metab* 2017;313:E167–E174.
- Teodoro JS, Rolo AP, Palmeira CM. Hepatic FXR: key regulator of whole-body energy metabolism. *Trends Endocrinol Metab* 2011;22:458–466.
- Walters JRF, Tasleem AM, Omer OS, Brydon WG, Dew T, le Roux CW. A new mechanism for bile acid diarrhea: defective feedback inhibition of bile acid biosynthesis. *Clin Gastroenterol Hepatol* 2009;7:1189–1194.
- Degen LP, Phillips SF. Variability of gastrointestinal transit in healthy women and men. *Gut* 1996;39:299–305.
- Guicciardi ME, Gores GJ. Bile acid-mediated hepatocyte apoptosis and cholestatic liver disease. *Dig Liver Dis* 2002;34:387–392.
- Liu J, Lu H, Lu Y-F, Lei X, Cui YJ, Ellis E, Strom CS, Klaassen DC. Potency of individual bile acids to regulate bile acid synthesis and transport genes in primary human hepatocyte cultures. *Toxicol Sci* 2014;141:538–546.
- Al-Khaifi A, Straniero S, Voronova V, Chernikova D, Sokolov V, Kumar C, Angelin B, Rudling M. Asynchronous rhythms of circulating conjugated and unconjugated bile acids in the modulation of human metabolism. *J Intern Med* 2018;284:546–559.
- Dawson PA, Lan T, Rao A. Bile acid transporters. *J Lipid Res* 2009;50:2340–2357.
- Guyton JR, Goldberg AC. Bile acid sequestrants. In: *Clinical lipidology*. Elsevier, 2009:281–287. Available from: http://www.crossref.org/deleted_DOI.html. Accessed: October 24, 2019.
- Paumgartner G. Ursodeoxycholic acid in cholestatic liver disease: mechanisms of action and therapeutic use revisited. *Hepatology* 2002;36:525–531.
- Slijepcevic D, van de Graaf SFJ. Bile acid uptake transporters as targets for therapy. *Dig Dis* 2017;35:251–258.
- Schaap FG, Trauner M, Jansen PLM. Bile acid receptors as targets for drug development. *Nat Rev Gastroenterol Hepatol* 2013;11:55–67.
- Hofmann AF, Molino G, Milanese M, Belforte G. Description and simulation of a physiological pharmacokinetic model for the metabolism and enterohepatic circulation of bile acids in man. Cholic acid in healthy man. *J Clin Invest* 1983;71:1003–1022.
- Hofmann AF, Cravetto C, Molino G, Belforte G, Bona B. Simulation of the metabolism and enterohepatic circulation of endogenous deoxycholic acid in humans using a physiologic pharmacokinetic model for bile acid metabolism. *Gastroenterology* 1987;93:693–709.
- Molino G, Hofmann AF, Cravetto C, Belforte G, Bona B. Simulation of the metabolism and enterohepatic circulation of endogenous chenodeoxycholic acid in man using a physiological pharmacokinetic model. *Eur J Clin Invest* 1986;16:397–414.
- Guiastrennec B, Sonne D, Hansen M, Bagger JI, Lund A, Rehfeld JF, Alskär O, Karlsson MO, Vilsbøll O, Knop FK, Bergstrand M. Mechanism-based modeling of gastric emptying rate and gallbladder emptying in response to caloric intake: models of gastric and gallbladder emptying. *CPT Pharmacomet Syst Pharmacol* 2016;5:692–700.
- Sips FLP, Eggink HM, Hilbers PAJ, Soeters MR, Groen AK, van Riel NAW. In silico analysis identifies intestinal transit as a key determinant of systemic bile acid metabolism. *Front Physiol* 2018;9.
- Hamilton JP, Xie G, Raufman J-P, Hogan S, Griffin LT, Packard CA, Chatfield DA, Hagey LR, Steinbach JH, Hofmann AF. Human cecal bile acids: concentration and spectrum. *Am J Physiol Gastrointest Liver Physiol* 2007;293:G256–G263.
- Keren N, Konikoff FM, Paitan Y, Gabay G, Reshef L, Naftali T, Gophna U. Interactions between the intestinal microbiota and bile acids in gallstones patients: bile acid and microbiota in gallstones patients. *Environ Microbiol Rep* 2015;7:874–880.
- Mouzaki M, Wang AY, Bandsma R, Comelli EM, Arendt BM, Zhang L, Fung S, Fischer SE, McGilvray IG, Allard JP. Bile acids and dysbiosis in non-alcoholic fatty liver disease. *PLoS One* 2016;11:e0151829.
- Aranha MM, Cortez-Pinto H, Costa A, Moreira da Silva IB, Camilo ME, Carniero de Moura M, Rodrigues CMP. Bile acid levels are increased in the liver of patients with steatohepatitis. *Eur J Gastroenterol Hepatol* 2008;20:519–525.
- Angelin B, Björkhem I, Einarsson K, Ewerth S. Hepatic uptake of bile acids in man. Fasting and postprandial concentrations of individual bile acids in portal venous and systemic blood serum. *J Clin Invest* 1982;70:724–731.
- Northfield TC, McColl I. Postprandial concentrations of free and conjugated bile acids down the length of the normal human small intestine. *Gut* 1973;14:513–518.
- Al-Khaifi A, Rudling M, Angelin B. An FXR agonist reduces bile acid synthesis independently of increases in FGF19 in healthy volunteers. *Gastroenterology* 2018;155:1012–1016.
- Krag E, Phillips SF. Active and passive bile acid absorption in man. Perfusion studies of the ileum and jejunum. *J Clin Invest* 1974;53:1686–1694.
- Mekhjian HS, Phillips SF, Hofmann AF. Colonic absorption of unconjugated bile acids: perfusion studies in man. *Dig Dis Sci* 1979;24:545–550.
- Parks DJ. Bile acids: natural ligands for an orphan nuclear receptor. *Science* 1999;284:1365–1368.
- Walters JRF, Johnston IM, Nolan JD, Vassie C, Pruzanski ME, Shapiro DA. The response of patients with bile acid diarrhoea to the farnesoid X receptor agonist obeticholic acid. *Aliment Pharmacol Ther* 2015;41:54–64.
- Pomare EW, Heaton KW. The effect of cholecystectomy on bile salt metabolism. *Gut* 1973;14:753–762.

32. Vati Rana S, Kaur J. Effect of post-cholecystectomy on small intestinal bacterial overgrowth and orocecal transit time in gallstone patients. *Int J Dig Dis* 2016;2.
33. Roda E, Aldini R, Mazzella G, Roda A, Sama C, Festi D, Barbara L. Enterohepatic circulation of bile acids after cholecystectomy. *Gut* 1978;19:640–649.
34. Lundåsen T, Gälman C, Angelin B, Rudling M. Circulating intestinal fibroblast growth factor 19 has a pronounced diurnal variation and modulates hepatic bile acid synthesis in man. *J Intern Med* 2006;260:530–536.
35. Fiamoncini J, Yiorkas AM, Gedrich K, Rundle M, Alsters SI, Roeselers G, van der Broek TJ, Clavel T, Lagkouvardos I, Wopereis S, Frost G, van Ommen B, Blakemore AI, Daniel H. Determinants of post-prandial plasma bile acid kinetics in human volunteers. *Am J Physiol Gastrointest Liver Physiol* 2017;313:G300–G312.
36. Pattni S, Walters JRF. Recent advances in the understanding of bile acid malabsorption. *Br Med Bull* 2009; 92:79–93.
37. Thaiss CA, Zeevi D, Levy M, Zilberman-Schapira G, Suez J, Tengeler AC, Abramson L, Katz MN, Korem T, Zmora N, Kuperman Y, Biton I, Gilad S, Harmelin A, Shapiro H, Halpern Z, Segal E, Elinav E. Transkingdom control of microbiota diurnal oscillations promotes metabolic homeostasis. *Cell* 2014;159:514–529.
38. Eggink HM, Oosterman JE, de Goede P, de Vries EM, Foppen E, Koehorst M, Groen AK, Boelen A, Romijn JA, la Fleur SE, Soeters MR, Kalsbeek A. Complex interaction between circadian rhythm and diet on bile acid homeostasis in male rats. *Chronobiol Int* 2017; 34:1339–1353.
39. Ridlon JM. Bile salt biotransformations by human intestinal bacteria. *J Lipid Res* 2005;47:241–259.
40. Angelin B, Einarsson K, Hellström K. Evidence for the absorption of bile acids in the proximal small intestine of normo- and hyperlipidaemic subjects. *Gut* 1976; 17:420–425.
41. Trauner M, Boyer JL. Bile salt transporters: molecular characterization, function, and regulation. *Physiol Rev* 2003;83:633–671.
42. Bender S, Sauer H, Hoffmann D. Kinetics of bile acid metabolism in experimental blind loop syndrome. *Gut* 1975;16:927–931.
43. Vrieze A, Out C, Fuentes S, Jonker L, Reuling I, Kootte RS, van Nood E, Holleman F, Knaapen M, Romijn JA, Soeters MR, Blaak EE, Dallinga-Thie GM, Reijnders D, Ackermans MT, Serlie MJ, Knop FK, Holst JJ, van der Ley C, Kema IP, Zoetendal EG, de Vos WM, Hoekstra JB, Stroes ES, Groen AK, Nieuwdorp M. Impact of oral vancomycin on gut microbiota, bile acid metabolism, and insulin sensitivity. *J Hepatol* 2014;60:824–831.
44. Phillips SF. Fatty acid diarrhoea: relationships between diarrhoea and steatorrhoea. In: Rommel K, Goebell H, Böhmer R, eds. *Lipid absorption: biochemical and clinical aspects*. Dordrecht: Springer Netherlands, 1976:241–254.
45. Dawson PA. Bile acid metabolism. In: *Biochemistry of lipids, lipoproteins and membranes*. Elsevier, 2016: 359–389. Available at: <http://linkinghub.elsevier.com/retrieve/pii/B9780444634382000122>. Accessed: November 28, 2016.
46. Dawson PA, Karpen SJ. Intestinal transport and metabolism of bile acids. *J Lipid Res* 2015;56:1085–1099.
47. Meier Y, Eloranta JJ, Darimont J, Ismail MG, Hiller C, Fried M, Kullak-Ublick GA, Vavricka SR. Regional distribution of solute carrier mRNA expression along the human intestinal tract. *Drug Metab Dispos* 2007; 35:590–594.
48. Einarsson K, Ahlberg J, Angelin B, Björkhem I, Ewerth S. Portal venous bile acids in cholesterol gallstone disease: effect of treatment with chenodeoxycholic and cholic acids. *Hepatology* 1985;5:661–665.
49. Dupas J-L, Ho NFH, Hofmann AF. Absorption of unconjugated bile acids from the perfused jejunum of the anesthetized rat: structure-activity relationships and rate-limiting steps. *Lipids* 2018;53:465–468.
50. Carey MC, Small DM. The physical chemistry of cholesterol solubility in bile. Relationship to gallstone formation and dissolution in man. *J Clin Invest* 1978; 61:998–1026.
51. Jazrawi RP, Bridges C, Joseph AE, Northfield TC. Effects of artificial depletion of the bile acid pool in man. *Gut* 1986;27:771–777.
52. Dilger K, Hohenester S, Winkler-Budenhofer U, Bastiaansen BA, Schaap FG, Rust C, Beuers U. Effect of ursodeoxycholic acid on bile acid profiles and intestinal detoxification machinery in primary biliary cirrhosis and health. *J Hepatol* 2012;57:133–140.
53. Angelin B, Björkhem I, Einarsson K. Individual serum bile acid concentrations in normo- and hyperlipoproteinemia as determined by mass fragmentography: relation to bile acid pool size. *J Lipid Res* 1978;19:527–537.
54. Einarsson K, Reihner E, Ewerth S, Björkhem I. Serum concentrations of unconjugated and conjugated cholic acid in portal venous and systemic venous blood of fasting man. *Scand J Clin Lab Invest* 1989;49:83–91.
55. Duane WC, Ginsberg RL, Bennion LJ. Effects of fasting on bile acid metabolism and biliary lipid composition in man. *J Lipid Res* 1976;17:211–219.
56. Jeejeebhoy KN. Short bowel syndrome: a nutritional and medical approach. *CMAJ Can Med Assoc J* 2002; 166:1297–1302.

Received November 25, 2019. Accepted February 19, 2020.

Correspondence

Address correspondence to: Veronika Voronova, M&S Decisions 125167, Naryshkinskaya Alley, 5, Building 1, Moscow, Russian Federation. e-mail: Veronika.Voronova@msdecisions.ru; fax: +7(495)7975535.

CRedit Authorship Contributions

Veronika Voronova, PharmD (Conceptualization: Equal; Data curation: Equal; Formal analysis: Lead; Investigation: Lead; Writing – original draft: Lead) Victor Sokolov, MSc (Formal analysis: Supporting; Investigation: Supporting; Validation: Equal; Writing – original draft: Supporting) Amani Al-Khaifi, PhD (Data curation: Equal; Formal analysis: Equal; Writing – review & editing: Supporting) Sara Straniero, PhD (Formal analysis: Supporting; Writing – review & editing: Supporting) Chanchal Kumar, PhD (Funding acquisition: Supporting; Project administration: Equal; Writing – review & editing: Supporting) Kirill Peskov, PhD (Conceptualization: Supporting; Funding acquisition: Supporting; Project administration: Supporting; Supervision: Equal; Writing – original draft: Supporting) Gabriel Helmlinger, PhD (Project administration: Supporting; Supervision: Supporting; Writing – original draft: Supporting) Mats Rudling, MD, PhD (Conceptualization: Equal; Formal analysis: Supporting; Funding

acquisition: Supporting; Writing – review & editing: Equal) Bo Angelin, MD, PhD (Conceptualization: Equal; Formal analysis: Equal; Funding acquisition: Lead; Resources: Equal; Writing – review & editing: Lead).

Conflicts of interest

Chanchal Kumar and Gabriel Helmlinger are employees of AstraZeneca Pharmaceuticals and may own shares; Kirill Peskov is the owner of M&S Decisions, LLC, and Veronika Voronova and Victor Sokolov are employees of M&S Decisions, LLC, a modeling research consultancy contracted by AstraZeneca Pharmaceuticals; Bo Angelin serves as a consultant to Albireo

AB and has received unrelated grant support from Amgen. The remaining authors disclose no conflicts.

Funding

This work was supported by AstraZeneca Pharmaceuticals, the Swedish Heart-Lung Foundation, the Swedish Research Council, the Cardiovascular Program of Karolinska Institutet/Stockholm County Council, the Knut and Alice Wallenberg Foundation, Sultan Qaboos University (3791/2012), the Leducq Foundation, and the Russian Academic Excellence Project 5-100 program.